P-04-249

Oskarshamn site investigation

Borehole KSH02: Characterisation of matrix pore water (Feasibility Study)

Niklaus Waber, University of Bern

John Smellie, Conterra AB

April 2004

Svensk Kärnbränslehantering AB
Swedish Nuclear Fuel
and Waste Management Co
Box 5864
SE-102 40 Stockholm Sweden
Tel 08-459 84 00
+46 8 459 84 00
Fax 08-661 57 19
+46 8 661 57 19

ISSN 1651-4416
SKB P-04-249

Oskarshamn site investigation

Borehole KSH02: Characterisation of matrix pore water (Feasibility Study)

Niklaus Waber, University of Bern

John Smellie, Conterra AB

April 2004

Keywords: Drillcore, Matrix groundwater, Leaching, Diffusion, Chemical analyses.

Abstract

Three drillcore samples at depths of 785 m, 879 m and 997 m from borehole KSH02 have been characterised mineralogically and geochemically before being subject to different laboratory procedures to determine the chemistry of the *in-situ* interconnected pore space fluid/groundwaters. The results show that borehole KSH02 is chemically and isotopically stratified between 785 m and 997 m depth. Chloride concentrations appear to increase from about 5,000 mg/L to 7,100 mg/L and the pore water has different chlorine and strontium isotopic signatures.

A methodology has been established for use in site characterisation investigations.

Sammanfattning

Tre kärnborrhålsprover vid 785 m, 879 m och 997 m från kärnborrhålet KSH02 har karakteriserats mineralogiskt och geokemiskt innan övriga laboratoriemetoder utförts av den in-situ kemiska sammansättningen i lösningen/grundvattnet, i det sammankopplade porutrymmet. Resultaten visa att borrhålet KSH02 är kemiskt och isotopiskt stratifierat mellan 785 m och 997 m djup. Kloridconcentrationen verkar öka från ca 5 000 mg/L till 7 100 mg/L och porvattnet har olika klor och strontium isotop signaturer.

Metodologin har etablerats för tillämpning i platsundersökningar.

Contents

1 Introduction

The following document reports the performance and results from the Feasibility Study "Pore space groundwaters in low permeable crystalline rock in KSH02". KSH02 is a 1,001.11 m deep core drilled borehole within the Simpevarp site investigation area, Oskarshamn. The work was conducted according to the activity plan AP PS 400-03-013 (SKB internal controlling document). The data is reported to SICADA in field note no Simpevarp 61.

2 Objective and scope

The main objective of the feasibility study was to characterise *in-situ* interconnected pore space fluid/groundwater in low permeable rocks representative of the major lithological,types intercepted by the borehole.

The scope of the study involved:

- The sampling and preservation of suitable drillcore lengths during drilling;
- The mineralogical and geochemical characterisation of the drillcore samples;
- The characterisation of the accessible and inaccessible pore space fluid/groundwater;
- The extraction by diffusion of the accessible pore space fluid/groundwater from the drillcore samples.

3 Sample preparation and analytical methods

Immediately on arrival at the University of Bern, the drilllcore samples were cut by dry sawing into one full-diameter subsample used for the diffusion experiments. On the subsamples to be used for other pore water investigations, the rim of the core (~ 1 cm) was removed by chisel and hammer. This was done to exclude possible contamination by drilling fluid in this zone of the core, which got possibly disturbed by drilling activites, and to ensure maximum water saturation of the rock material. The wet weight of such material was determined immediately after preparation. The remaining rim material was further prepared for mineralogical and geochemical investigation.

Three samples were selected for study and the following investigations were performed.

1. **The mineralogy** was determined by optical microscopy of thin sections prepared from the core rim material. For the quantification of bulk mineralogy by X-ray diffractometry and bulk chemical analyses by X-ray fluorescence the remaining core rim material was crushed and milled to a grain size of < 63µ and homogenised. For the identification of the clay mineralogy the grain size fraction < 2µ was separated by sedimentation.
2. **Bulk density (ρ_{bulk})** was determined on subsamples of about 1 cm^3 from the core centre by the Hg-displacement method. The sample cube was then ground to < 60µm and the grain density (ρ_{grain}) measured by He-pycnometry.
3. **The water content** was determined by weighing the subsamples from the core centre immediately after preparation followed by drying at 105ºC until stable weight conditions (±0.002 g). The water content was determined by drying the subsamples a second time after re-saturation. Re-saturation was achieved by immersion of the material into distilled water for 2 to 7 days depending on the size of the subsamples. For both states the water-content porosity was calculated from the water loss and the grain density measured by He-pycnometry. Comparison of these two obtained water-content porosity values yields the degree of saturation of the samples at the time the samples were received. Water-content measurements were also conducted on the subsamples used for the diffusive-exchange method and the diffusion experiments.
4. **Fluid inclusion petrography and microthermometry** were conducted using a Linkham THMSG-600 heating-cooling stage with a Linkham TMS 91 temperature control on a Leitz Orthoplan microscope equipped with a 100/0.75 M Plan objective lens. Laser Raman micro-spectroscopy was performed using a LabRam HR 800 Confocal-laser Raman microprobe with a frequency-doubled Nd-YAG laser. The Raman microprobe is equipped with an Olympus BX41 microscope with a Nikon 100/0.75 M Plan objective lens and a Linkham MDS-600 heating-cooling stage with a Linkham TMS 94 temperature. Measurement conditions were a laser beam at 532.12 nm, a hole width of 400µm, a slit of 100µm, and an accumulation time of 3x40 secs. The relative abundance of fluid inclusions was determined by image analysis of individual quartz grains.
5. **Aqueous leaching tests** were performed on different grain-size fractions prepared from the centre material of subsample E from core KSH02-879. Leaching was performed in double-distilled water by shaking the PE tubes end over end for 24 hours under ambient conditions. Measurements of pH and alkalinity (by titration) were determined immediately after termination of the experiment. Major cations and anions were determined by atomic adsorption spectrometry at the University of Bern and ion chromatography at Hydroisotop GmbH, respectively, with a relative error of ± 5%.

6. **The stable water isotope composition** of the pore water was determined by the diffusive equilibration method as described by /Rogge, 1997/, /Rübel, 2000/ and /Rübel et al. 2002/. In this method the isotope exchange occurs through the gaseous phase without any direct contact between the rock sample and the test water. Rock pieces of about 1 cm in diameter from the centre of the core, and a small petri dish filled with a known mass of test water of known $\delta^{2}H$ and $\delta^{18}O$ values, were stored together in a vapour-tight glass container. In the test water about 0.3 mol NaCl were dissolved to lower the water vapour pressure above the test water surface, thus avoiding the loss of test water from the petri dish and condensation on the rock fragments and the glass container walls. The dish, including the test water as well as the whole container, was weighed before and after the equilibration experiment to check that no water is lost from the container and there was no transfer of test water to the sample by possible swelling of the rock material. Equilibrium in the three reservoir system - rock samples, test water, and the air inside the container as diaphragm - was achieved in about 10 to 30 days at room temperature depending on the size and water content of the rock pieces. After complete equilibration the test water was removed and analysed by ion-mass spectrometry at Hydroisotop GmbH.
7. **Diffusion experiments** were performed on complete core samples of about 80 mm in height by immersion in double-distilled water enriched in ^{16}O and ^{1}H. The vapour-tight teflon containers were stored under controlled temperature in a dark place. At regular intervals a small sample (about 1.5 ml) was taken for chloride analysis by ion-chromatography using a 0.2 µL injection loop at the University of Bern. After steady-state with respect to chloride was achieved, the chemical composition, pH, and alkalinity of the diffusion experiment test solutions were determined by the same methods as used for the aqueous extract solution at Hydroisotop GmbH.
8. **The isotopic compositions of oxygen and hydrogen** in the various test solutions (aqueous extracts, diffusive equilibration method, and diffusion experiments) were determined by conventional ion-ratio mass spectrometry at Hydroisotop GmbH. The results are reported relative to the V-SMOW standard with a precision of ± 0.15‰ for $\delta^{18}O$ and ± 1.5‰ for $\delta^{2}H$. The $^{87}Sr/^{86}Sr$ isotope ratio was measured at the University of Bern using a modified VG Sector® thermal ionisation mass spectrometer (TIMS) in simple collector mode, using oxidised Ta filaments. The analytical uncertainty is given with 2σ of multiple measurements of the same sample. Total Sr concentrations are given in ppm. The $^{37}C1/^{35}C1$ isotopic ratios, expressed as $\delta^{37}C1$ relative to SMOC, were measured at the University of Waterloo Environmental Isotope Lab (EIL) using a VG SIRA 9 Mass Spectrometer. Measurements were made with a precision of ± 0.15% (1σ) based on repeat analyses of SMOC.

4 Results

The three samples come from depth intervals around 785 m, 879 m, and 997 m (Table 2-1). For legibility reasons the sample labelling adopted in this report is the full metre lengths along the drillcore with the borehole name as prefix, i.e. KSH02-785, KSH02-879, KSH02-997. The capital letter behind this sample number is indicative for the experiment/ analytical investigation performed on a subsample of the drillcore sample received. The full analytical programme performed on the samples is given in Table 4-1.

Table 4-1. Borehole KSH02: samples, subsamples and investigations performed.

Experiment/investigation	KSH02-785	KSH02-879	KSH02-997
SKB no	005337	005342	005337
Depth Interval	785.30–785.52	879.29–879.53	997.01–997.26
Diffusion-experiment	A	A	A
Isotope diffusive equilibration experiment	B	B	B
Water content and water-content porosity	C	C	C
Grain and bulk density, physical porosity	D	D	D
Aqueous extractions of different grain-size fractions	–	E	–
Fluid inclusion investigations	F	F	F
Mineralogy, chemistry	G	G	G

4.1 Rock composition

4.1.1 Mineralogical composition

The three rock samples are of dark grey-bluish colour with a fine-grained matrix (≤ 1 mm) and phenocrysts between about 3–5 mm. All have a well preserved magmatic texture with no obvious metamorphic overprint such as a preferential lineation and/or extensive deformation features in individual minerals. In all three samples the contents of quartz and feldspars amount to about 60 wt %, while the relative contribution of mafic and opaque minerals varies slightly (Table 4-2). In the QAP-diagram the rock compositions plot on the boundary between typical granodioritic and monzodioritic composition (Figure 4-1). According to the regional mapping protocol the major rock type from borehole KSH02 is considered to be a fine-grained dioritoid. Compared to typical Ävrö granite and quartz monzodiorite compositions (i.e. Äspö diorite) from the Äspö HRL, they are depleted in quartz and enriched in plagioclase.

Sample KSH02-785 has a fine-grained matrix (0.1–0.4mm) mainly comprising xeno-morphic to hypidiomorphic quartz and hypidiomorphic to idiomorphic K-feldspar and plagioclase, the latter being of albite-rich composition. This matrix contains phenocrysts of K-feldspar, plagioclase, amphibole and biotite. Phenocrysts of K-feldspar quite frequently occur as perthite, show twinning and some of them display a granophyric texture. Sericitisation of K-feldspar is only poorly developed and haematite staining is completely absent. The plagioclase phenocrysts are anorthite-rich in composition, often display growth-zonation and only slight saussuritisation. Amphibole phenocrysts are hypidiomorphic to idiomorphic and appear to be of hornblende composition. In parts they replace pyroxene

and are altered at the rims to biotite, chlorite and opaque mineral phases. Pyroxene is finely dispersed throughout and has a grain size intermediate between the matrix and the phenocrysts. The hypidiomorphic to idiomorphic crystals appear to be of augitic composition and are often altered on the rims to biotite, chlorite and opaque mineral phases. Biotite occurs as a deuteric alteration product and as irregular, large flakes up to 5 mm. It has abundant radiation haloes from inclusions of zircon and sphene and shows partly weak chloritisation. Further characteristic for this sample is its high content of opaque phases of mainly illmenitic and magnetitic composition.

Samples KSH02-879 and KSH02-997 differ from the above sample in that they have higher contents in plagioclase and pyroxene, but lower contents in K-feldspar and opaque phases (Figure 4-1, Table 4-2). In these samples the fine-grained matrix is mainly composed of well preserved, idiomorphic and An-rich plagioclase laths together with hypidiomorphic quartz. As in sample KSH02-785, saussuritisation of plagioclase and sericitisation of K-feldspar is rare. Phenocrysts of amphibole (probably hornblende) dominate over pyroxene, which appears to be of augitic composition. Deuteric alteration of these minerals to biotite, chlorite and opaque phases is less pronounced than in sample KSH02-785. Similarly, biotite in the matrix and as phenocrysts has a fresh appearance and chloritisation is only poorly developed. The content of opaque phases is lower in these samples compared to sample KSH02-785. Accessory minerals include in all samples sericite, chlorite, sphene, zircon, monazite, apatite and very few clay minerals.

In comparison to the rocks of the Äspö HRL, the absence of any oxidising hydrothermal alteration leading to the typical reddish staining due to haematite pigmentation in KSH02 is most prominent. In addition, the abundant occurrence of amphibole, pyroxene and opaque phases distinguishes these rocks from those of the Äspö HRL.

Table 4-2. Mineralogical composition of investigated samples (wt % from XRD analysis, vol % from thin section analysis)

Borehole	**Unit**	**KSH02**	**KSH02**	**KSH02**
Sample		**785 G**	**879 G**	**997 G**
Depth		**785.30–785.52**	**879.28–879.53**	**997.01–997.26**
Quartz	wt %	12	16	14
K-feldspar	wt %	20	19	14
Plagioclase	wt %	28	34	32
Pyroxene	vol %	1–5	5–10	5–10
Amphibole	vol %	10–15	15–20	10–15
Biotite	vol %	15–20	5–10	15–20
Opaque Phases	vol %	5–10	1–5	1–5
Calcite	wt %	0.6	0.9	< 0.5
Accessories	Chlorite, sericite, clay minerals (very few), apatite, monazite, sphene, zircon			

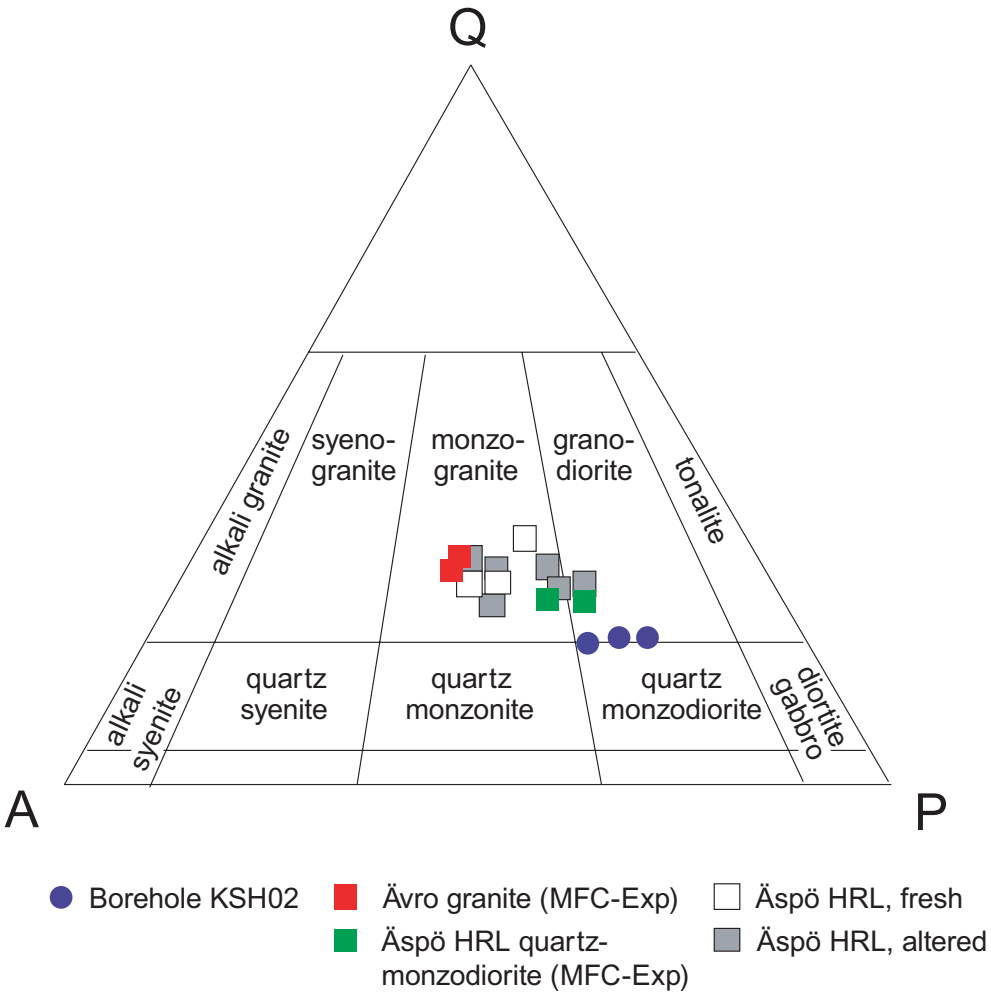

Figure 4-1. *Modal distribution of quartz, alkali feldspar and plagioclase (QAP) of the samples from borehole KSH02 in comparison with crystalline rocks from the Äspö HRL /data from Eliasson, 1993/ and from the Matrix Fluid Chemistry Experiment (MFC-Exp), /Smellie et al. 2003/.*

4.1.2 Chemical composition

The chemical composition of the rock samples from borehole KSH02 is given in Table 4-3 and graphically represented in Figures 4-2 and 4-3. With SiO_2 contents of < 60 wt %, these samples from borehole KSH02 are more basic than most of the rocks of the Äspö HRL area; they are further characterised by lower concentrations of Al, Na, Ba, Zn, and Zr than the Äspö HRL rocks. In contrast, they have higher contents in K, Fe, Mg, Ca, Ti, Sr, Ni, and Nb. The relatively high contents of metallic elements such as Ti, Cr, Cu, Ni, and Pb have to be attributed to the presence of opaque phases (illmenite, magnetite and pyrite). X-ray diffraction and microscopic analysis did not reveal a single Ba or Sr mineral phase and these elements appear to be associated mainly with feldspars and, for Sr, eventually with trace amounts of calcite.

The chemical composition is consistent with the mineralogical analysis, and normative calculations according to the CIPW-norm support the quartz monzodiorite compositions obtained from the mineralogical investigations (Figure 4-1).

Table 4-3. Chemical composition of investigated samples (analysis by X-ray fluorescence)

Borehole	Unit	KSH02	KSH02	KSH02
Sample		785 G	879 G	997 G
Depth (m)		785.30–785.52	879.28–879.53	997.01–997.26
SiO_2	wt %	58.90	57.46	58.06
TiO_2	wt %	0.95	0.95	1.02
Al_2O_3	wt %	15.53	15.73	16.24
Fe_2O_3	wt %	7.20	6.60	7.53
MnO	wt %	0.12	0.11	0.12
MgO	wt %	3.38	2.45	2.70
CaO	wt %	5.38	5.17	5.64
Na_2O	wt %	2.91	3.22	3.02
K_2O	wt %	3.71	3.68	3.04
P_2O_5	wt %	0.27	0.29	0.30
LOI	wt %	0.40	0.54	0.67
SUM	wt %	99.05	96.49	98.64
Ba	ppm	915	868	782
Cr	ppm	81	19	8
Cu	ppm	< 2	26	8
Nb	ppm	14	13	14
Ni	ppm	25	11	13
Pb	ppm	30	20	36
Rb	ppm	98	102	77
Sr	ppm	593	597	594
V	ppm	< 5	< 5	< 5
Y	ppm	22	20	22
Zn	ppm	93	89	88
Zr	ppm	218	201	188

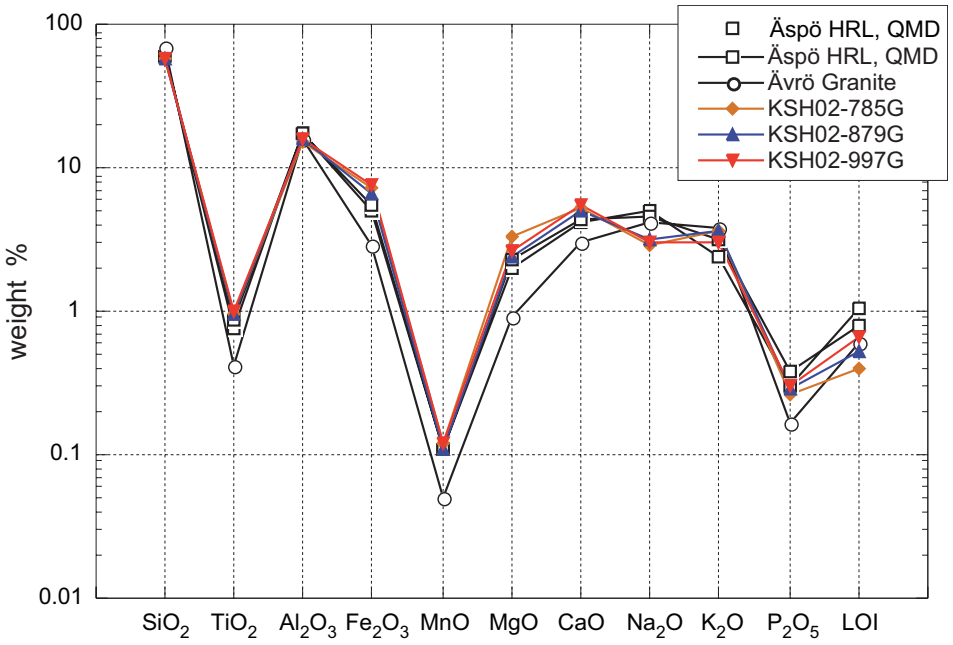

Figure 4-2. *Major element composition of samples from borehole KSH02 compared to the Äspö HRL quartz monzodiorite (QMD) and Äspö HRL Ävrö granite from the MFC-Experiment /Smellie et al. 2003/. (LOI: loss on ignition).*

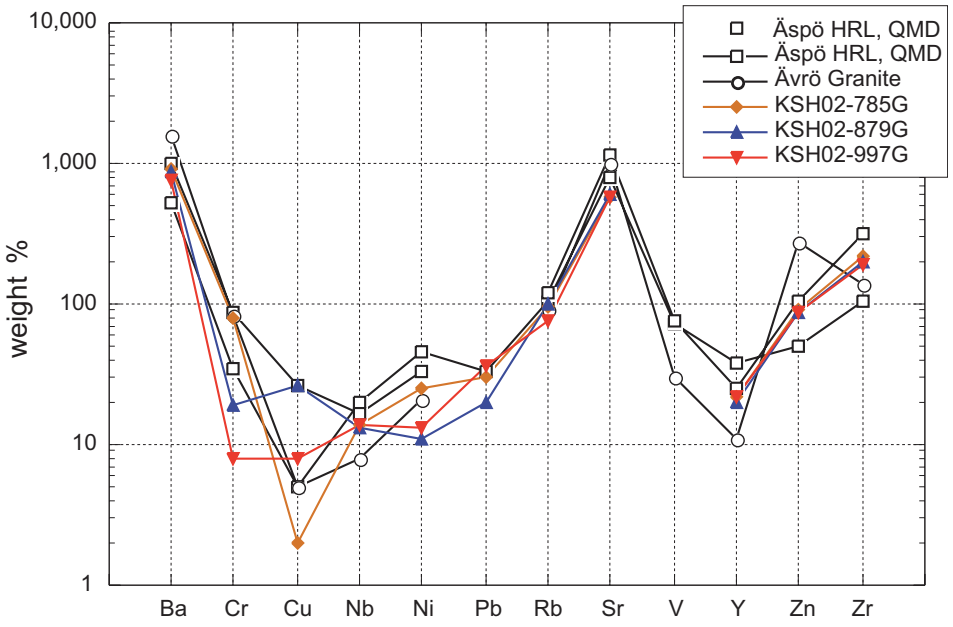

Figure 4-3. *Trace element composition of samples from borehole KSH02 compared to the Äspö HRL quartz monzodiorite (QMD) and Äspö HRL Ävrö granite from the MFC-Experiment /Smellie et al. 2003/.*

4.2 Petrophysical measurements

The characterisation of pore water in rocks of very low permeability and low water content requires the knowledge of the water-accessible porosity. This is simply because the pore water in such rocks cannot be sampled directly, but has to be accessed by indirect methods, which all include a dilution of the *in-situ* pore water present. Extensive reviews of this problem and of presently available techniques with their respective advantages and drawbacks are given in /Pearson, 1999; Sacchi and Michelot, 2000; Sacchi et al. 2001; Pearson et al. 2003a/ and /Smellie et al. 2003/.

Petrophysical measurements conducted on the drillcore samples from borehole KSH02 include bulk and grain density by Hg-displacement and He-pycnometry, respectively, and the determination of the water loss by drying at 105°C. From the so obtained values the different types of porosity were calculated. The definitions and nomenclature of the different types of porosity follows those given in /Smellie et al. 2003/ in that the *physical porosity* describes the ratio of total void volume to the total volume of rock, the *connected porosity* is described by the water-content porosity obtained from gravimetric water-loss measurements, and the *diffusion porosity* is determined by diffusion experiments.

Perturbation of porosity values measured in the laboratory from those present in-situ have two major origins besides the analytical uncertainty. These are desaturation of the core sample during sample recovery and handling, and stress release of the sample due to the retrieval from great depth. Desaturation was investigated by re-saturating the samples in distilled water and comparing the two water-loss measurements, and the determination of the saturation state of the samples. The influence of stress release was investigated by the isotope diffusive-exchange method, which reveals a water-content porosity independent of stress release and, under favourable conditions, a diffusion porosity.

4.2.1 Bulk density, grain density and physical porosity

The physical porosity, Φ_{Phys}, of a rock can be calculated from measurements of bulk and grain density according to

$$\Phi_{Phys} = [\ 1-(\rho_\beta / \rho_\gamma] \qquad (1)$$

where ρ_β is the bulk density and ρ_γ is the grain density.

As shown in Table 4-4, measured bulk and grain densities for the KSH02 core subsamples are identical within the analytical error and consequently the calculated physical porosity is of low accuracy. This becomes also evident by comparison of the obtained physical porosity with the water-content porosity (see Section 3.2.2). In reality the physical porosity should be at least as high as the water-content porosity because it includes beside the connected pore space also isolated pores in the rock matrix and in minerals (i.e. fluid inclusions). This is not the case for the KSH02 core subsamples as can be seen from Tables 3-3 and 3-4. Improvement could be achieved by a higher accuracy of the analytical techniques and measurements of multiple samples for a statistical approach to allow for rock heterogeneity.

Table 4-4. Bulk density, grain density and physical porosity.

Borehole		KSH02	KSH02	KSH02
Sample		785 C2	879 C2	997 C2
Depth (m)		785.30–785.52	879.28–879.53	997.01–997.26
Bulk density	g/cm³	2.801	2.798	2.763
Grain density	g/cm³	2.802	2.801	2.766
Physical porosity	%	0.005	0.108	0.100

4.2.2 Connected porosity from water-loss measurements

The water loss of KSH02 core subsamples was determined gravimetrically by drying the samples at 105°C until stable weight conditions. The drying time varied between 168 and 360 hours depending on the sample size. The water-content porosity, Φ_{WC}, was then calculated using the measured grain density and based on the wet weight of the sample according to:

$$\Phi_{WC} = \frac{WC_{wet} \cdot \rho_{grain}}{WC_{wet} \cdot \rho_{grain} + (1 - WC_{wet}) \cdot \rho_{water}} \quad (2)$$

The *degree of saturation*, S, is the ratio of water-filled to total pore space accessible for water, (V_{wat}/V_{pores}), and the *volumetric moisture content*, θ, is the ratio of water-filled pore space to total volume (V_{wat}/V_{tot}). Degree of saturation and volumetric moisture content are thus related by:

$$\theta = S \times \Phi_{Phys} \quad (3)$$

As can be seen from the water contents measured after being received (Table 4-5), five subsamples of the three KSH02 core samples agree fairly well. Exceptions are subsamples 785C1 and 997A. The lower water content measured for subsample 785C1 can be related to the small rock mass used which can lead to an increased analytical error during weighing. For sample 997A the higher water content might be related to the formation of a small hair fissure during the long-term experiment due to stress release. The average water-content porosity calculated for the three samples after reception varies between 0.096% and 0.170%. This is thus higher than the physical porosity obtained from bulk and grain density measurements, except for sample KSH02-879. This underlines the low accuracy of the latter porosity values.

Sample series A and C were afterwards subjected to re-saturation by immersion in distilled water. For the volumetrically large A-samples this re-saturation took place during the diffusion experiment and lasted 113 days. The small-sized pieces (max 1 cm in diameter) of the C-samples were re-saturated during 72 hours before they were dried and weighed once more. This time, a stable weight was reached after 240 hours. Between the A- and C-subsample series the water content after re-saturation is equal for sample KSH02-879, but differs by about 25% and 100% for samples KSH02-785 and KSH02-997, respectively (Table 4-5). In both cases stress release in the volumetrically large A-subsamples appears to be the reason for this discrepancy. This is, for example indicated by the above mentioned hair fissure that formed in sample KSH02-997A and which continuously increased during the diffusion experiment. *Therefore, the water-content porosity values for these samples were perturbed by stress release, were not representative for in-situ conditions and were not used for further interpretation.*

Table 4-5. Water content by drying, water content porosity and degree of saturation.

Sample KSH02	Experiment	Rock mass as received	Drying		Sample as received		Sample re-saturated		Degree of saturation
			Temp	Time	Water content	Water content porosity	Water content	Water content porosity	
		(g)	(°C)	(hour)	(%)				
785 A	Diffusion-exp	448.80	105	360	0.053	0.150	0.102	0.287	52.2
785 B LAB	Isotope-exch	76.47	105	168	0.051	0.143			
785 B SSI	Isotope-exch	76.47	105	168	0.056	0.156			
785 C1	Water-content	56.85	105	192	0.035	0.099	0.070	0.197	50.0
785 C2	Water-content	71.52	105	192	0.056	0.157	0.084	0.235	66.7
Average KSH02-785					0.050 ± 0.009	0.141 ± 0.024	0.085 ± 0.016	0.240 ± 0.045	
879 A	Diffusion-exp	420.38	105	360	0.033	0.092	0.124	0.341	27.0
879 B LAB	Isotope-exch	98.81	105	168	0.040	0.109			
879 B SSI	Isotope-exch	98.81	105	168	0.034	0.095			
879 C1	Water-content	83.44	105	192	0.036	0.099	0.120	0.331	30.1
879 C2	Water-content	95.64	105	192	0.031	0.087	0.115	0.317	27.3
Average KSH02-879					0.035 ± 0.003	0.096 ± 0.008	0.120 ± 0.005	0.330 ± 0.012	
997 A	Diffusion-exp	407.21	105	360	0.093	0.261	0.147	0.411	63.4
997 B LAB	Isotope-exch	99.26	105	168	0.047	0.133			
997 B SSI	Isotope-exch	99.26	105	168	0.049	0.138			
997 C1	Water-content	96.19	105	192	0.062	0.175	0.073	0.204	85.7
997 C2	Water-content	97.41	105	192	0.051	0.144	0.062	0.172	83.3
Average KSH02-997					0.060 ± 0.019	0.170 ± 0.053	0.068 ± 0.008	0.188 ± 0.23	

All samples were significantly desaturated after being received in the laboratory. The reasons for this were inadequate sealing of the samples at the drill site (the bags were no longer evacuated), and the time interval between core recovery, packing and delivery of the core samples to the laboratory was too long. The pore water loss from the time of core retrieval to the laboratory was more than 70% for sample KSH02-879, almost 50% for sample KSH02-785 and about 15% for sample KSH02-997. Obviously this has large consequences on all other experimental investigations and inhibits an accurate derivation of an in-situ pore water composition.

To guarantee more successful experimental data in future investigations, priorities have to be set to precisely follow the previously submitted sampling protocol and to deliver the core samples within one to two days to the laboratory.

4.3 Fluid inclusion studies

The composition and abundance of fluid inclusions were investigated to evaluate the potential contribution of inclusion fluid to the salinity of the pore water. As shown in the Matrix Fluid Chemistry Experiment at the Äspö HRL such investigation are mandatory for a correct interpretation of indirect methods of pore water characterisation that involve disintegration of rock samples /Smellie et al. 2003/. In core samples retrieved from great depth rupture of fluid inclusions might be induced by stress release (in addition to those inclusions opened during the drilling process) and thus potentially perturb experiments performed on intact core samples such as diffusion experiments.

In the fine-grained dioritoid samples of borehole KSH02 fluid inclusions occur almost exclusively in quartz. Therefore, microthermometric and Raman-spectrometric fluid inclusion investigations focussed on inclusions in quartz only. The full analytical dataset including photographic documentation and Raman spectra of inclusions is given in the Appendix.

4.3.1 Morphology, texture and abundance of quartz

Sample KSH02-785 is characterised by a fine-grained matrix that consists of quartz and feldspar. Most of the quartz in this sample has a grain size of < 1 mm and zones with coarser grained quartz are rare. The individual quartz grains show only weak undulous extinction under polarised light and there is no obvious anisotropy developed in the quartz texture. In the rock matrix of samples KSH02-879 and -997 quartz occurs as more coarse-grained in type, but shows otherwise the same characteristics as in sample KSH02-785.

All samples display a magmatic texture with only weak indications of deformation. Recrystallisation of quartz as very fine-grained equigranular subcrystals around larger crystals, the occurrence of secondary fluid inclusions along healed fissures in quartz, and the partial chloritisation of biotite, are all indications for a deuteric and/or hydrothermal overprint of the rocks.

The quartz content was estimated from image analyses of about 200 images per sample. This allowed the derivation of a rather accurate volumetric content of quartz for the more coarse-grained samples, while for the fine-grained sample KSH0-785 only a range could be estimated (Table 4-6). The so obtained quartz contents compare well with those derived by X-ray diffraction, which delivered a quartz content in wt % (Table 4-2).

Table 4-6. Quartz content from image analysis of thin sections.

Borehole	Unit	KSH02	KSH02	KSH02
Sample		785 F1	879 F1	997 F1
Depth (m)		785.30–785.52	879.28–879.53	997.01–997.26
Quartz	vol %	15–20	10.5	13.5

4.3.2 Fluid inclusion populations

In the fine-grained dioritoid samples quartz contains two main groups of fluid inclusions. Type I contains single-phase liquid-only and two-phase liquid-vapour inclusions and Type II contains single-phase gas-only inclusions. Type I inclusions can be further subdivided according to their salinity (see Section 4.3.3)

Single-phase, liquid-only inclusions of Type I are of secondary origin and occur mainly along healed fissures in quartz. In these metastable inclusions the gas/vapour bubble cannot nucleate below the solvus and the homogenisation temperature appears to be below about 120°C. Commonly, this population occurs in intimate association with two-phase inclusions of Type I and it can be assumed that the salinity of the single-phase, liquid-only inclusions is similar to that of the associated two-phase inclusions.

Two-phase, liquid-vapour inclusions of Type I are of secondary origin also, and occur mainly along healed fissures in quartz. The gas/vapour bubbles in these inclusions vary from 0% to (i.e. single-phase) to almost 100% within the same inclusion association along a healed fissure. The salinity of these inclusions, however, is independent of the size of the gas/vapour bubble. This allows the above conclusion that the liquid-only inclusions have the same salinity as two-phase inclusions within the same inclusion association. The difference in the size of the gas/vapour bubble is most probably due to necking-down features of the inclusions and not due to fluid separation. These necking-down features inhibit the measurement of petrologically meaningful homogenisation temperatures and thus homogenisation temperatures were not measured.

Type II inclusions are gas-only inclusions that contain no liquid phase. They might be of primary origin, although more detailed petrographic investigations would be required to support this hypothesis. From physical-chemical considerations, however, it appears unlikely that the vapour-only inclusions are genetically associated with the liquid-bearing Type I inclusions. In the present study Type II inclusions were only identified in sample 997F. This does not, however, imply that such inclusions are not present in the other two fine-grained dioritoid samples.

Microthermometric and Raman-spectrometric investigations of Type II inclusions reveal that the gas composition is almost pure CO_2 with only minor amounts of N_2 (Table 4-7; see also Appendix, Table A3). In some of these inclusions gas clathrate $CO_2 \times 7.5H_2O$ was observed. For others, petrographic evidence revealed that they were overprinted by the highly saline secondary fluid of the neighbouring two-phase inclusions.

For the purpose of pore water characterisation these Type II inclusions are less important, although they might form an additional source of CO_2 in destructive experiments. However, despite their low abundance, the CO_2 in the inclusion is under high pressure and thus the amount of CO_2 present might become recognisable in some experiments (cf Chapter 5).

Table 4-7. Gas compositions of gas-only Type II inclusions present in sample 997F.

Sample	FI Number	Type	Tm CO_2 (°C)	X_{CO2} (fraction)	X_{N2} (fraction)
997 F	3.0.4	II	–56.6	0.989	0.011
997 F	3.0.5	II	–56.7	0.953	0.047
997 F	3.0.7	II	–57.9	0.935	0.065
997 F	3.0.17	II	–56.6	0.992	0.008

Tm HH = range of melting temperature of hydrohalite ($NaCl \times 2H_2O$).

Mass ratio = $(NaCl)/(NaCl+CaCl_2)$.

4.3.3 Salinity

The two-phase Type I inclusions cover a salinity range from about 0.5 eq wt % NaCl to more than 25 eq wt % NaCl, based on the microthermometric measurements. Figures 4-4 and 4-5 summarise the final melting temperature of ice and the derived salinity expressed as eq wt % NaCl of the more than 100 investigated inclusions. The complete data of the individual measurements on fluid inclusion is given in the Appendix (Tables A1 to A3).

Based on their salinity the Type I inclusions can be further subdivided (Table 4-8). This subdivision is arbitrary, but allows some statements about the abundance of saline inclusions and thus the possibility of inclusion fluid contributing to the pore water salinity. In sample 785 F inclusions of Types Ia, Ib and Ic were found with the low-salinity inclusions of Type Ia being the least abundant (Figure 4-5). Sample 879 F contains mainly inclusions of Type Ib and few low-salinity inclusions of Type Ia. High-salinity inclusions of Type Ic were not identified in this sample. As mentioned above sample 997 F is the only sample were gas-only inclusions (Type II) were identified. Of the liquid-bearing inclusions the low-salinity Type Ia and the high-salinity Type Ic inclusions dominate, while Type b inclusions are almost absent.

Hase such as halite was not observed in any of the fluid inclusions, but hydrohalite ($NaCl \times 2H_2O$) was observed in the more saline inclusions of Type Ib and Ic. The occurrence of hydrohalite was also confirmed by Raman spectrometry (see Appendix). No other hydrates such as of $CaCl_2$, $MgCl_2$ or $FeCl_2$ could be detected with Raman spectrometry. However, it is well known that the spectra of hydrohalite and antarcticite ($CaCl_2 \times 6H_2O$) overlap and are difficult to distinguish, while others are easily identified. In many of the inclusions the decomposition temperature of hydrohalite is significantly decreased. This decrease must be due to another salt, which can only be $CaCl_2$ due to the absence of easily identifiable other salts. Based on phase relationships the amount of $CaCl_2$ present in these inclusions can be calculated to be between about 1.8 wt % and 16.3 wt % (Table 4-9).

Table 4-8. Salinity ranges of two-phase Type I inclusions.

Inclusion type	Salinity	Tm ice [1)]
	eq wt % NaCl	°C
Ia	0–6	0 to –3.7
Ib	6–12	–3.7 to –9.1
Ic	13–25	< –9.1

[1)] Tm ice: final ice melting temperature.

Table 4-9. Salt composition of two-phase Type I inclusions.

Sample	FI Number	Type	Tm HH °C	NaCl wt %	$CaCl_2$ wt %	Total Salt wt %	Mass Ratio
785 F	1.1.6	Ic	–27	7.5	9.2	16.7	0.45
			–28	5.8	10.9	16.7	0.35
785 F	2.0.9	Ib	–26	7.8	1.8	9.6	0.82
			–27	4.4	5.4	9.8	0.45
785 F	3.1.2	Ic	–24	18.4	1.7	20.1	0.92
			–25	17.5	2.5	20.0	0.87
879 F	1.3.16	Ib	–26	5.6	1.3	6.9	0.82
			–27	3.2	3.9	7.1	0.45
997 F	3.6.23	Ic	–31	5.1	15.9	21.0	0.24
			–32	4.6	16.3	20.9	0.22

Tm HH = range of melting temperature of hydrohalite ($NaCl \times 2H_2O$), mass ratio = $(NaCl)/(NaCl+CaCl_2)$.

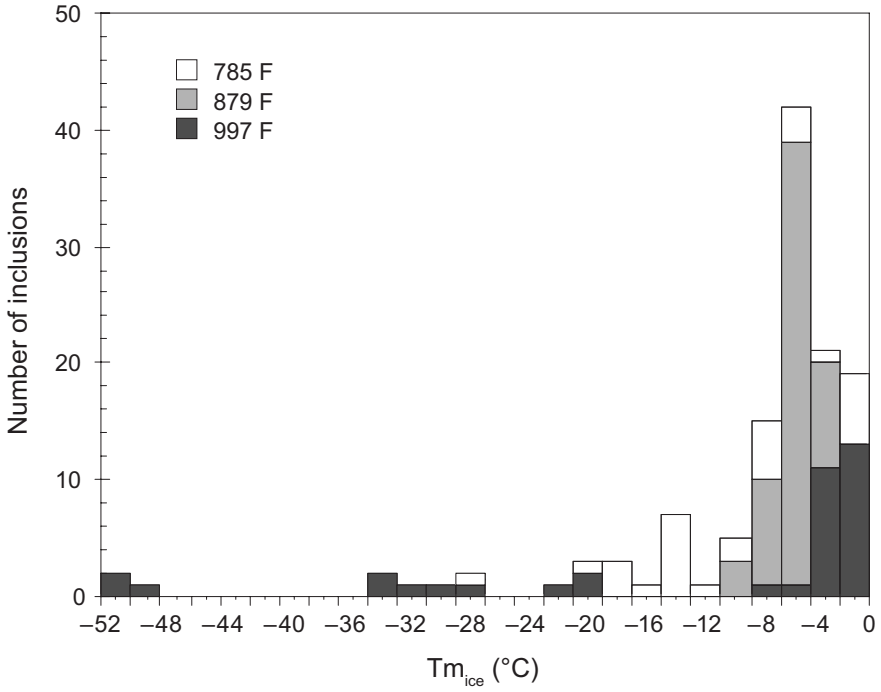

Figure 4-4. *Distribution of final ice melting temperature derived from microthermometric measurements of fluid inclusions in quartz from KSH02 borehole fine-grained dioritoid samples.*

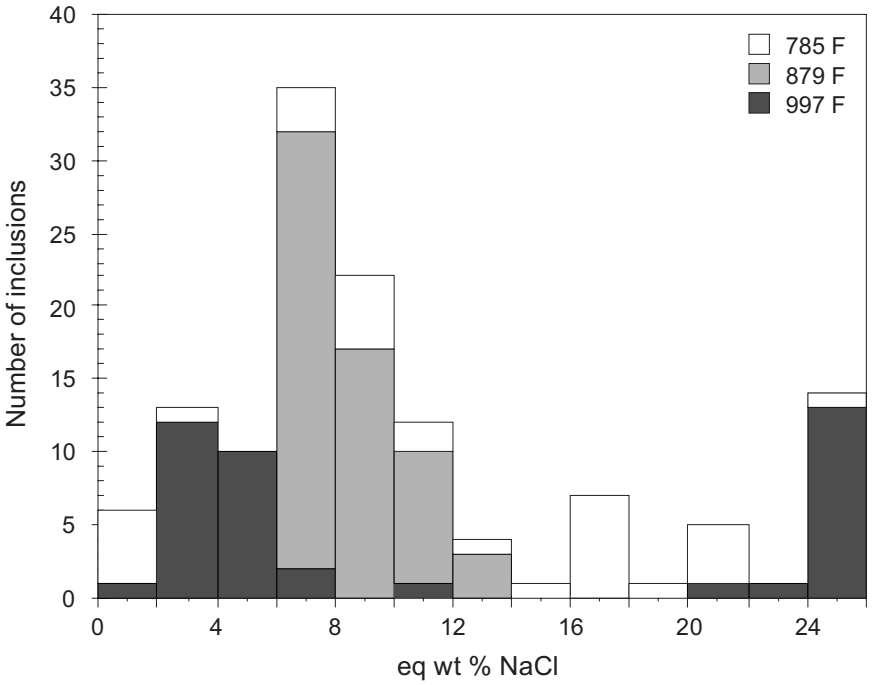

Figure 4-5. *Distribution of salinity expressed as eq wt % NaCl derived from microthermometric measurements of fluid inclusions in quartz from KSH02 borehole fine-grained dioritoid samples.*

4.3.4 Abundance of fluid inclusions

More than 100 inclusions have been investigated for their composition in the three drillcore samples. The selection made was based on the different compositional types of inclusions rather than develop a sound statistic of the individual inclusion types. Therefore, the distribution given in the previous section of differently saline inclusions might not be very representative. Nevertheless, it appears that in all rock samples abundant moderately to highly saline inclusions occur.

To estimate the total abundance of fluid inclusions in quartz of the fine-grained dioritoid samples, about 20 quartz grains were investigated by image analysing techniques. The inclusion density varies between 0 and 5 vol % from quartz grain to quartz grain. As an average, fluid inclusions consist about 0.5 to 1 vol % of the total quartz volume in the rocks of borehole KSH02.

5 Rock pore water studies

Pore water that resides in the pore space between minerals and along grain boundaries in crystalline rocks of low permeability cannot be sampled by conventional groundwater sampling techniques and has to be characterised by applying indirect methods based on drillcore material. Such techniques have been tested during the Matrix Fluid Chemistry Experiment in the Äspö HRL /Smellie et al. 2003/.

In the present feasibility study on drillcore material of the KSH02 borehole the experimental approaches to characterise the pore water chemistry involved aqueous leaching experiments, pore water diffusion, and the diffusive-exchange method for stable water isotopes. This last method was not tested before in the Äspö HRL, but is regarded as important because it also delivers a measure of water content that is independent of the commonly applied gravimetric water-content determinations. For the other two methods applied the experimental and analytical protocol has been modified and expanded according to the lessons learned from the Matrix Fluid Chemistry Experiment.

5.1 Aqueous leaching experiments

Aqueous leaching experiments were conducted only on subsample E from core sample KSH02-879. Before crushing and grinding the material used from the central part of the core was dried at 40°C. During drying dissolved constituents in the pore water will precipitate as highly soluble salts following complex evaporation cycles. Crushing and grinding of the rock material will additionally liberate fluid trapped in mineral fluid inclusions. The mineralisation of a leachate solution is thus the sum of: 1) the constituents originally dissolved in the pore water, 2) the constituents present in inclusion fluid, and 3) water-rock interaction during the leaching process.

The current study focussed on aqueous leaching of five different grain-size fractions. The largest two grain-size fractions (> 4 mm and 2–4 mm) were chosen to be slightly above and in the range of the average grain size of the KSH02-879 fine-grained dioritoid sample. The next two fractions (0.83–2 mm and 0.14–0.83 mm) are representative for the grain size of the fine-grained rock matrix, while in the most fine-grained fraction (< 63 µm) essentially all minerals are destroyed. The aim of the experiment was: 1) to explore the impact of inclusion fluid on the leach solution, 2) to explore the impact of water-rock interaction during leaching in the coarse-grained fraction for comparison with the diffusion experiment, and 3) to allow a certain statement to be made about the changes of the pore water composition in the near-vicinity of a future rupture zone underground without (i.e. coarser-grained fractions) and with (i.e. fine-grained fractions) the development of a fault gouge.

Chemical and isotopic data of the aqueous leaching experiments including the data calculated for the carbonate system are given in Table 5-1. The results for dissolved Na and K analysed in two different laboratories agree well within the analytical error giving confidence to the remaining chemical data. Note that for the two most coarse-grained fractions the data given correspond to a solid:liquid ratio of 2:1 used in the experiment. For comparison with the other extract solutions, these concentrations have to be divided by a factor of 2, which is, however, strictly only applicable to chemically conservative elements. The isotope data are directly comparable because these are ratios and not absolute concentrations.

All dissolved cation and anion concentrations increase with decreasing grain size (Figures 5-1 and 5-2). The increase is particularly large for Cl and Na indicating the increasing salt contribution from crushed fluid inclusions to the fine-grained fractions. *This indicates that salts from fluid inclusions will significantly perturb all pore water investigations based on rock material that involve crushing of the rock material.* The Na/Cl ratio of around 2 obtained in the leach solutions further suggests that mineral dissolution reactions take place during leaching because a Na/Cl ratio of around 1 could be expected if the NaCl-dominated fluid inclusion salts would be the only salt source besides the pore water (cf Chapter 4). Alternatively, the pore water itself might have a Na/Cl ratio above unity. This latter hypothesis is supported by the solution composition of the diffusion experiments which show even higher Na/Cl ratios (cf Section 5.3).

A similarly strong but more irregular increase in concentration with decreasing grain size is obtained for K and SO_4 (Figures 5-1 and 5-2). In the extract solution 879 E5 of the most fine-grained fraction, the concentrations of K and SO_4 are more than twice the corresponding concentrations in the other extract solutions. Fluid inclusion investigations revealed no measurable concentrations for these components in the inclusion fluid. Therefore, the origin of these components is the dissolution during extraction of K-feldspar and possibly biotite for potassium and of pyrite for sulphur. In comparison to the solution composition of the diffusion experiments the K/Na and the SO_4/Cl ratios are higher in the aqueous extract solutions (cf Section 5.3).

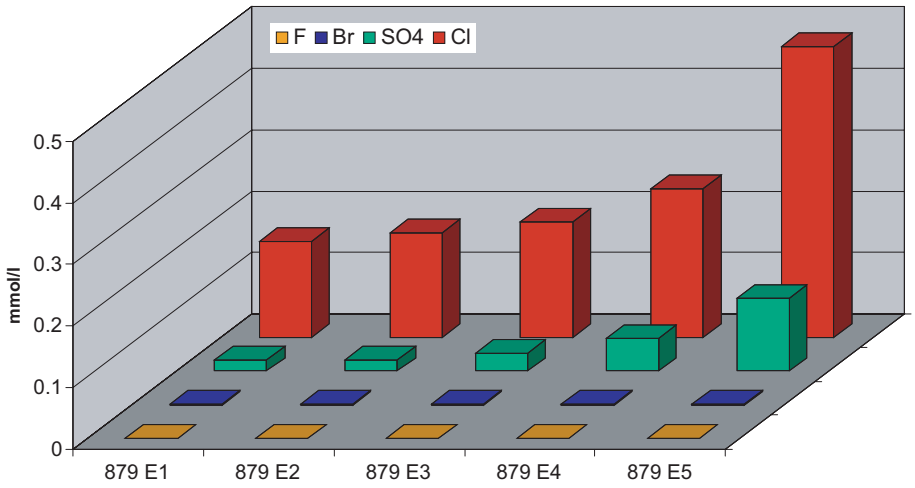

Figure 5-1. *Anion concentrations in aqueous leach solutions of different grain-size fractions of sample KSH02-879E (solid:liquid ratio 1:1; grain size: E1 = > 4 mm, E2 = 2–4 mm, E3 = 0.83–2 mm, E4 = 0.14–0.83 mm, E5 < 63µm).*

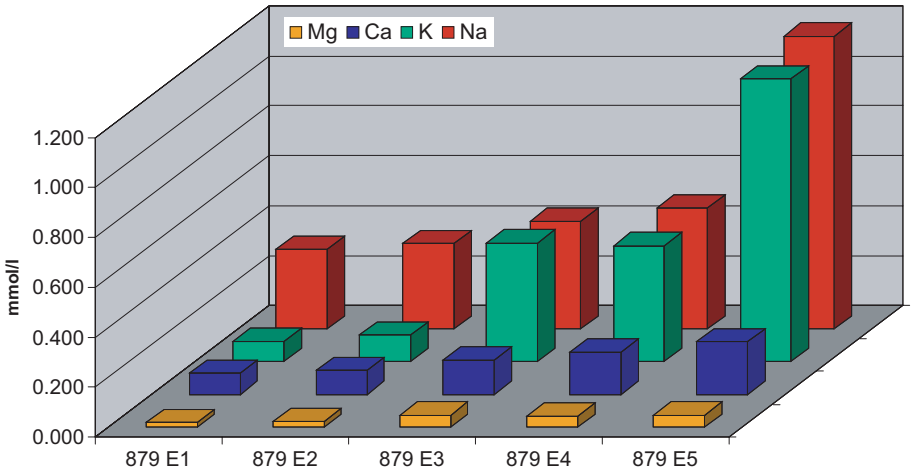

Figure 5-2. *Cation concentrations in aqueous leach solutions of different grain-size fractions of sample KSH02-879E (solid:liquid ratio 1:1;grain size: E1 = > 4 mm, E2 = 2–4 mm, E3 = 0.83–2 mm, E4 = 0.14–0.83 mm, E5 < 63µm).*

The concentration of Ca also increases with decreasing grain size, while that of Mg remains about constant. All rock samples contain small amounts of calcite as an alteration product of the observed saussuritisation (Table 4-2) and the extract solutions are at equilibrium with calcite or even supersaturated with respect to calcite (Table 5-1). The comparison of the molar concentrations of Ca and TIC reveals that in the extract solution 879 E1 to 879 E4 the TIC is about four times higher, while it is eight times higher than the Ca concentration in the extract solution 879 E5 of the most fine-grained fraction. Neither the distilled water used in the experiments, which was initially in equilibrium with the atmosphere (TIC ~ 1.3×10^{-5} mol), nor continuous equilibration with the atmosphere during the experiment (this would results in a log pCO_2 of about –3.5 compared to the calculated ones of about –4.4) can fully account for the analysed TIC. This suggests other carbon sources in the rock such as CO_2 in fluid inclusions and in the original pore water.

The comparison of the ratios of Na/Cl, K/Na, and SO_4/Cl in the aqueous extract solutions from different grain-size fractions and the solutions obtained from the diffusion experiment (Tables 5-1 and 5-5) reveals that mineral dissolution reactions are more prominent in the aqueous extraction test. The reason for that are the newly created, much larger reactive surface areas and an aqueous extract solution far from equilibrium with the rock. In the diffusion experiment, in contrast, such contact is strongly limited and the initial solution, i.e. the pore water, can be expected to be in equilibrium with the rock. Based on that it can be concluded that the *in-situ* pore water has a Na/Cl ratio above unity and Cl is not the only dominating anions.

Table 5-1. Chemical, isotopic, and modelling data of aqueous extraction tests of different grain-size fractions (sample KSH02-879).

Sample description						
Borehole		**KSH02**	**KSH02**	**KSH02**	**KSH02**	**KSH02**
Sample		879 E1	879 E2	879 E3	879 E4	879 E5
Type of sample		Aq Extract	Aq Extract	Aq Extract	Aq Extract	Aq Extract
Laboratory analytics		HI/UniBe	HI/UniBe	HI/UniBe	HI/UniBe	HI/UniBe
Laboratory extract		UniBe	UniBe	UniBe	UniBe	UniBe
Extraction date		Nov 03	Nov 03	Nov 03	Nov 03	Nov 03
Conditions extraction		ambient	ambient	ambient	ambient	ambient
Extraction time		24 hours	24 hours	24 hours	24 hours	24 hours
S:L ratio		2:1	2:1	1:1	1:1	1:1
Grain size		> 4 mm	2–4 mm	0.83–2 mm	0.14–0.83 mm	> 63 µm
Miscellaneous properties						
pH (lab)	–log(H+)	8.96	8.97	9.05	9.06	9.33
Sample temperature	ºC	20	20	20	20	20
Dissolved constituents						
Cations						
Sodium (Na^+), UniBe	mg/l	12.7	14.1	9.3	11.2	28.0
Potassium (K^+), UniBe	mg/l	5.9	7.6	18.2	18.5	42.2
Sodium (Na^+)	mg/l	14.6	14.1	9.9	11.1	26.9
Potassium (K^+)	mg/l	6.4	8.4	18.6	18.1	44.2
Magnesium (Mg^{+2})	mg/l	1.0	1.1	1.2	1.1	1.2
Calcium (Ca^{+2})	mg/l	6.7	7.7	5.5	6.8	8.4
Strontium (Sr^{+2})	mg/l	< 0.2	< 0.2	< 0.2	< 0.2	< 0.2
Anions						
Fluoride (F^-)	mg/l	< 1	< 1	< 1	< 1	< 1
Chloride (Cl^-)	mg/l	11.1	12.1	6.7	8.6	16.8
Bromide (Br^-)	mg/l	< 2	< 2	< 2	< 2	< 2
Sulphate (SO_4^{-2})	mg/l	3.5	3.6	2.9	5.1	11.4
Nitrate (NO_3^-)	mg/l	< 1	< 1	1.9	1.2	1.7
Total alkalinity	meq/l	0.7	0.8	0.9	0.9	1.8
Tot Alkalinity as HCO_3	mg/l	42.7	48.8	54.9	54.9	109.8
Parameters calculated from analytical data						
Sum of anal. constit	mg/l	89	100	102	107	220
Charge Balance:	%	+3.80	+4.41	+4.05	+4.07	+5.22
Ion-Ion ratios						
Na/Cl molal	mol/mol	2.028	2.001	2.279	1.990	2.469
K/Na molal	mol/mol	0.523	0.629	2.517	1.908	2.386
SO_4/Cl molal	mol/mol	0.116	0.110	0.160	0.219	0.250
Carbonate system						
Calculated using measured values						
TIC from alkalinity	mol/kg	6.620e-04	7.555e-04	8.434e-04	8.409e-04	1.602e-03
Calcite saturation index		–0.05	0.07	0.05	0.14	0.68
log $p(CO_2)$		–4.39	–4.35	–4.38	–4.40	–4.42
Isotopes						
$\delta^{37}Cl$ (‰ V-SMOC)		3.62 *		6.83 *		1.48 ± 0.15
$^{87}Sr/^{86}Sr$		0.724505		0.771355		0.749042
$^{87}Sr/^{86}Sr$ error		0.00033		0.00012		0.000042

* value not reliable due to too small amount of Cl.

The Sr-isotope ratios in the aqueous extract solution differ significantly and are more radiogenic in the extract solutions of more fine-grained grain-size fractions (Table 5-1). This is consistent with higher proportions of mineral dissolution (mainly feldspars) in these fractions as observed from the chemical composition of the extract solutions. The $^{87}Sr/^{86}Sr$ ratio of the extract solution 879 E1 from the most coarse grained grain-size fraction is within the analytical error identical to the solution of the diffusion experiment of the same core sample (cf Tables 5-1 and 5-5).

The measured Cl-isotope ratios of extract solutions 879 E3 and, although to a lesser degree 879 E1, are, according to the laboratory, not trustworthy due to the low total Cl concentrations in the samples and the resulting small Cl-isotope peaks during mass-spectrometric measurement. The $\delta^{37}Cl$ value of extract solution 879 E5 of the most fine-grained fraction is, within the analytical error, almost identical to that obtained for the solution of the diffusion experiment (cf Tables 5-1 and 5-5). This could suggest that the isotopic composition of Cl in the fluid inclusion is not very different from that of the *in-situ* pore water.

5.2 Isotopic composition of pore water by diffusive exchange

5.2.1 Background

The diffusive-exchange method for the determination of the stable water isotope composition and the water content of low-permeability rocks was developed by /Rogge, 1997/ and /Rübel, 2000/ at the Institut für Umweltphysik, IUP, University of Heidelberg, Germany. The need for this new technique stemmed from the observation that the previously applied vacuum-distillation technique was often inaccurate due to incomplete distillation and associated Rayleigh-distillation effects during the experiment /Araguàs-Araguàs et al. 1995; Moreau-Le Golvan et al. 1997; Sacchi and Michelot, 2000/ and the difficulties attached to the determination of the water content by gravimetric methods in evaporite-mineral bearing rocks and clay-rich rocks /Rogge, 1997; Pearson et al. 2003b/. Up to the present, the diffusive-exchange method was applied to clay-rich rocks with water contents of more than 3 wt % and a few evaporites with water contents as low as 0.5 wt %. The present study is the first time that this method was applied to crystalline rocks with very low water contents of below 0.15 wt %.

By applying the diffusive-exchange method several aspects have to be considered /Rogge, 1997; Rübel, 2000; Rübel et al. 2002/:

First, the response time τ of the system to completely equilibrate the test water and the pore water has to be determined. This is most favourably done from the temporal evolution of either the δ^2H or $\delta^{18}O$ values of the test water by equilibrating several subsamples over different periods of time. Alternatively, the response time τ can be estimated from the relationship:

$$\tau_{total} = \mu / R_{total} \quad (4)$$

where μ is the characteristic mass derived from ratio of mass of test water to mass of pore water and R_{total} denotes the total exchange rate according to:

$$R_{total} = [d^2_{test}/(D_{water} \times m_{tw}) + d^2_{pw}/(D_{water} \times m_{pw}) + 1_{air}/(D_{air} \times \rho_{air} \times A_{air}) \quad (5)$$

where d = distance between the surface of the test water and the surface of the most distant rock piece, D = diffusion coefficient, m = mass, r = density, A = cross-section area, tw = test water, and pw = pore water. This latter approach had to be chosen in the present study because the available mass of rock material from the central part of the cores (to ensure maximum saturation) was limited to less than 100 g. For the KSH02 core samples the response time τ estimated from equation (5) is about one day. To ensure full equilibration between test water and pore water the experiments were run for 20 days.

To minimise condensation on the rock pieces and/or the container walls salt is added to the test water. Thus, one has to consider a difference in the salinity between test water and pore water that results in a slight difference in isotope content of both reservoirs. While there is almost no effect on ^{18}O, the liquid-vapour equilibrium fractionation factor of Deuterium is dependent on salinity /Horita et al. 1993/. The systematic effect on the result at room temperature is about 2.7‰ × ΔM in δ^2H, where ΔM denotes the difference in molality between solutions. For the KSH02 core samples the difference in salinity is less than about 10 g/L (cf Section 5.3) and the absolute error of the δ^2H value resulting from this salinity effect is thus lower than 1‰.

The stable isotope composition of the pore water and the water content of the sample are calculated from mass balance relationship of the experiments according to:

$$m_{pw} \times c_{pw}\big|_{t=0} + m_{tw} \times c_{tw}\big|_{t=0} = \left(m_{pw} + m_{tw}\right) \times c_{tw}\big|_{t=\infty} \qquad (6)$$

where m = mass, c = isotope concentration, pw = pore water, tw = test water and the concentrations on the left side of the equation are prior to equilibration (t = 0), while the concentration on the right side is after equilibration is achieved (t = ∞) in the experiment. Each equilibration experiment reveals two independent equations of the type (6) for $\delta^{18}O$ and δ^2H. To enable the calculation of the three unknowns, $\delta^{18}O$ and δ^2H of the pore water and the pore water mass (i.e. the water content), two different exchange experiments have to be performed for each sample to receive the necessary four equations. It should be noted that by complete equilibration the mass balances remain correct even if a small amount of test is transferred to the sample during the experiment.

By applying Gauss' law of error propagation /Rogge, 1997/ and /Rübel, 2000/ showed that the error of the equilibration experiment for the determination of the isotope composition of the pore water increases with the difference in isotopic composition between test water and pore water. On the other hand, the error of the equilibration experiment for the determination of the water content decreases with the difference in isotopic composition between test water and pore water. Therefore, to minimise the analytical error: a) a test water with $\delta^{18}O$ and δ^2H values close to that expected for the pore water was used for the determination of the isotopic composition, and b) a test water with $\delta^{18}O$ and δ^2H values far from that expected for the pore water was used for the determination of the water content. In the present experiment this was achieved by using laboratory supply water ($\delta^{18}O$ = –10.82‰, δ^2H = –76.4‰) and melt water from an Antarctic ice core (SSI-DYE, $\delta^{18}O$ = –26.96‰, δ^2H = –205.8‰).

5.2.2 Results

The results of the diffusive-exchange experiments performed with rock material from the KSH02 core are summarised in Table 5-2. In this table the "Sample-Lab" and "Sample-SSI" designate the experiments performed with laboratory supply water and Antarctic melt water, respectively. The isotope composition of the test water before and after complete equilibration is labelled "initial" and "final", respectively.

Table 5-2. Results of the diffusive-exchange experiments to derive the stable isotope composition and the water content of the pore water. Some of the calculated isotope values (in italics) are unrealistic and only poor agreement is obtained with gravimetric water content measurements (see text for explanation).

Sample	Lab test water	Sample -LAB		Light test water	Sample -SSI		Pore water	
	Mass	Initial $\delta^{18}O$	Final $\delta^{18}O$	Mass	Initial $\delta^{18}O$	Final $\delta^{18}O$	Water content	$\delta^{18}O$
	(g)	(‰ V-SMOW)		(g)	(‰ V-SMOW)		(%)	(‰ V-SMOW)
785 B	5.02	–10.81	–10.76	5.03	–26.96	–26.55	*0.138*	*–8.57*
879 B	5.04	–10.81	–10.76	5.03	–26.96	–26.50	*0.099*	*–1.37*
997 B	5.05	–10.81	–10.72	5.06	–26.96	–26.34	*0.177*	*–8.07*

Analytical error $\delta^{18}O$: ± 0.15‰.

Sample	Lab test water	Sample -LAB		Light test water	Sample -SSI		Pore water	
	Mass	Initial $\delta^{2}H$	Final $\delta^{2}H$	Mass	Initial $\delta^{2}H$	Final $\delta^{2}H$	Water content	$\delta^{2}H$
	(g)	(‰ V-SMOW)		(g)	(‰ V-SMOW)		(%)	(‰ V-SMOW)
785 B	5.02	–76.4	–74.9	5.03	–205.8	–202.6	*0.801*	*37.4*
879 B	5.04	–76.4	–76.6	5.03	–205.8	–200.6	*0.236*	*–81.2*
997 B	5.05	–76.4	–76.1	5.06	–205.8	–200.7	*0.200*	*–68.3*

Analytical error $\delta^{2}H$: ± 1.5‰.

Evaluation of the data given in Table 5-2 reveals that there is only poor agreement between the water contents calculated using the diffusive-exchange method and those obtained from gravimetric measurements. Also, there is a non-systematic pattern between the water contents calculated from the oxygen isotope experiments and those calculated with the hydrogen isotopes. From equation (6) it becomes obvious that the mass of pore water needs to be known accurately in order to calculate the isotope composition of the pore water. The lack of such accurate data is the main reason for the non-systematic pattern obtained for the stable isotope composition of the pore water of the three samples. It appears that some process must have altered the isotopic composition of the pore water from the time of core recovery to the time of the laboratory experiments. An indication for this process is given by the oxygen and hydrogen isotope compositions of samples 879B and 785B, respectively, both being unrealistically enriched in the heavy isotopes.

Enrichment in ^{18}O and ^{2}H of the water phase occurs, for example, during evaporation. Thus, the main reason for these inaccurate results is the poor degree of saturation of only about 30% to 80% of the core samples when received at the laboratory (cf Section 4.2.2). Desaturation of the rock is the result of pore water evaporation under open system conditions. Under such conditions, the isotopic composition of the pore water is changed according to a Rayleigh-distillation where the remaining pore water gets continuously enriched in the heavy isotope according to

$$R = R_0 f^{(\alpha - 1)} \tag{7}$$

where R_0 = the initial isotope ratio, R = the isotope ratio when only a fraction (f) remains, and a = the fractionation factor between the liquid and the vapour phase.

Figure 5-3 illustrates the enrichment in heavy isotopes of the remaining pore water during evaporation as a function of the fraction of water remaining in the rock sample. It can be seen that the effect is large (especially for hydrogen) if the remaining fraction becomes less than about 80%, which approximately corresponds to the best preserved sample received.

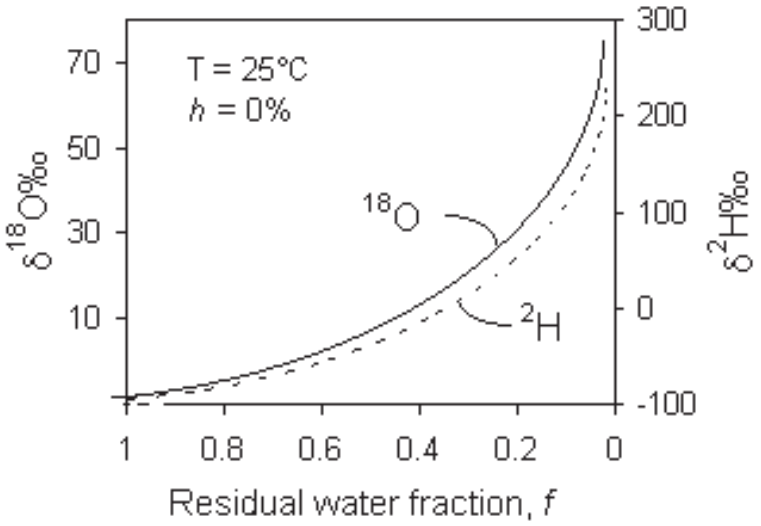

Figure 5-3. *Enrichment of ^{18}O and ^{2}H in distilled water during evaporation of water under controlled conditions at a humidity, h, of 0% and a temperature of 25°C. As the fraction of water remaining approaches 0, a Rayleigh distillation causes an exponential increase in the heavy isotopes. Under conditions of increasing humidity, exchange with the vapour phase reduces the exponential enrichment. Under conditions of high humidity, a steady state value is reached due to complete exchange with the vapour mass /from Clark and Fritz, 1997/.*

Another important factor for the inaccuracy of the calculated water content and pore water isotope values is the fact that the isotope compositions of the test water before and after equilibration overlap within the analytical precision (Table 5-2). While also an effect of desaturation, this can be improved upon in future experiments by adjusting the mass of pore water (i.e. saturated rock mass) and that of the test water to a more favourable ratio and to improve the analytical precision for the hydrogen isotope measurements.

To conclude, the diffusive-exchange method has been successfully applied to crystalline rocks with a very low water content. Although the results are not representative for the current samples, the reasons have been identified and correspondingly the protocol will be changed for future experiments.

5.3 Diffusion experiments

Diffusion experiments on drillcore samples from borehole KSH02 were conducted to derive: 1) the composition of chloride and possible other conservative elements, and 2) to evaluate the dominant mineral reactions during such experiments. Information from both of these approaches would be required for modelling the *in-situ* pore water composition. Because chloride can be expected to be one of the dominant anions in the pore water, the calculation of the measured Cl content to an *in-situ* Cl content utilising an accurate pore

water content measure will give the necessary information about the ionic strength of the *in-situ* pore water as required for modelling. Similarly, the observed dominant mineral reactions in the experiment would help to constrain the model input.

5.3.1 Set-up experiments

Diffusion experiments were performed on full core diameter samples that were conditioned at the top and the bottom by dry cutting immediately after being received. The sample parameters used in these experiments are summarised in Table 5.3. The semi-quantitative bulk density calculated from the measured weight and volume is in fair agreement with the actual density measurements (Tables. 5-3 and 4-4). As noted in Section 4.2.2, the degree of saturation was about 52% for sample 785A, 27% for sample 879A , and 63% for sample 997A. Sample 997A developed a hair fissure during the experiment due to stress release. This has further perturbed the water content measurements and to a certain degree possibly the chemical data, too.

In the diffusion experiments a steady state situation was reached with respect to chloride after about 100 days (Table 5-4, Figure 5-4). As can be seen from Table 5-3 the ratio of pore water in the rock to experimental test water is very small. Therefore, in the calculations of the *in-situ* Cl concentration (see Section 5.4) the small amount of Cl present in the rock after termination of the experiment lies within the analytical error and can be neglected in a first assumption.

Table 5-3. Sample parameters as used for the diffusion experiment.

Parameter	Unit	785 A	879 A	997 A
Rock weight as received	g	448.80	420.38	407.21
Rock volume (semi-quantitative)	cm^3	161.29	151.49	147.06
Rock density (semi-quantitative)	g/cm^3	2.78	2.77	2.76
Rock weight after experiment	g	449.02	420.76	407.43
Uptake of water	mL	0.22	0.38	0.22
Rock weight after drying	g	448.56	420.24	406.90
Initital volume of test water	mL	123.68	134.18	116.60
Subsample volume for 4 Cl analyses	mL	6.72	6.62	6.53
Final volume of test solution	mL	116.75	127.19	109.85
Volume pore water (re-saturated)	mL	0.46	0.52	0.60
Ratio pore water/test solution	mL	0.004	0.004	0.005

5.3.2 Chemical composition

The chemical data of the diffusion experiments are given in Table 5-5 and graphically illustrated in Figure 5-5. The test solutions of the three samples show a similar total mineralisation between 109 mg/L and 133 mg/L. This total mineralisation is the sum of the amount of dissolved solids added from the rocks pore water and mineral dissolution reactions that took place during the experiment. With respect to the major element distribution in the test solutions, samples 785A and 997A show a similar pattern except for F^- (Figure 5-5). Test solution 879 A, however, displays a considerably different picture and has higher contents of K, Ca, Cl and SO_4, but a lower Na content.

Table 5-4. Chloride time series of diffusion experiment solutions.

Sample description				
Borehole		**KSH02**	**KSH02**	**KSH02**
Sample		785 A	879 A	997 A
Interval		785.30–785.52	879.28–879.53	997.01–997.26
Rock type		Fine-grained dioritoid	Fine-grained dioritoid	Fine-grained dioritoid
Type of sample		Diff-ex solution	Diff-ex solution	Diff-ex solution
Laboratory analytics		HI/UniBe	HI/UniBe	HI/UniBe
Laboratory experiment		UniBe	UniBe	UniBe
Start experiment		Aug 06, 2003	Aug 06, 2003	Aug 06, 2003
End experiment		Nov 28, 2003	Nov 28, 2003	Nov 28, 2003
Experiment time	days	113	113	113
Date	**Δ days**	**Cl (mg/L)**	**Cl (mg/L)**	**Cl (mg/L)**
September 03, 2003	28	11.5	23.4	13.3
September 23, 2003	48	13.1	22.2	15.3
October 20, 2003	75	15.4	23.0	15.6
October 31, 2003	85	15.4	23.9	16.2
November 28, 2003	113	15.9	24.7	17.0

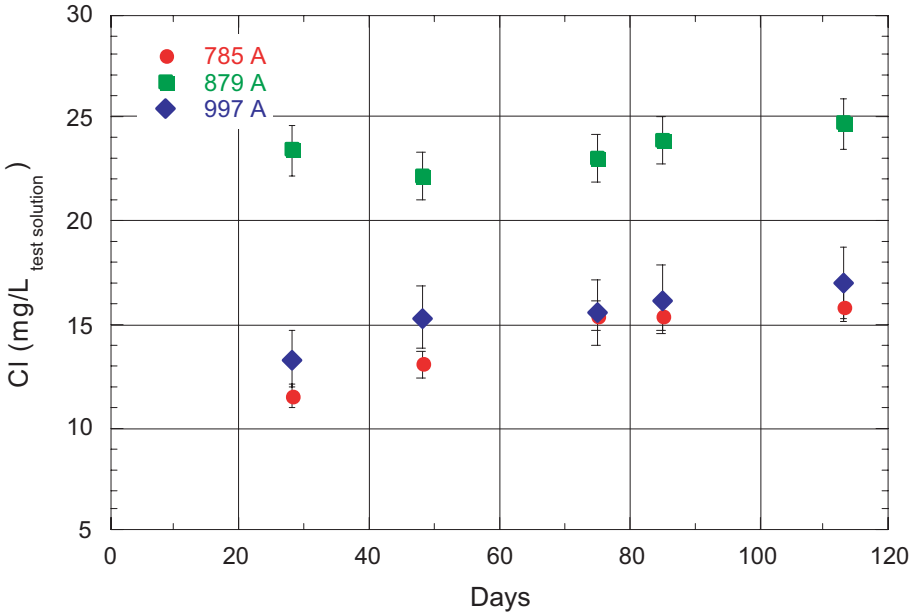

Figure 5-4. *Evolution of Cl concentration in the test solution as a function of diffusion time. For all samples a steady-state was achieved within the analytical uncertainty after about 100 days. The last sample (133 days) was used for complete chemical and isotopic analyses; the first four samples are subsamples of less than 2 mL and were used only for Cl analyses.*

Based on the mineralogy of the granodiorite samples and the dissolution reaction rates under ambient conditions /Sverdrup, 1990/ the following sequence of minerals contributing to the mineralisation of the test water can be established:

Sulphides, calcite > anorthite-rich plagioclase >> quartz, amphibole (hornblende) > K-feldspar, albite-rich plagioclase, pyroxene (augitic) > biotite.

Based on the similar mineralogy, the same water-rock ratio, and the same diffusion time used in the experiment, it could be expected that in all samples the contribution from mineral dissolution reactions is about the same. Large differences in the test solution composition could then be related to differences in the pore water composition. This assumption implies that the water accessible porosity and thus the accessible reactive mineral surface area are about the same. Unfortunately, this cannot be further evaluated due to the known uncertainty related to water content due to desaturation of the rock samples.

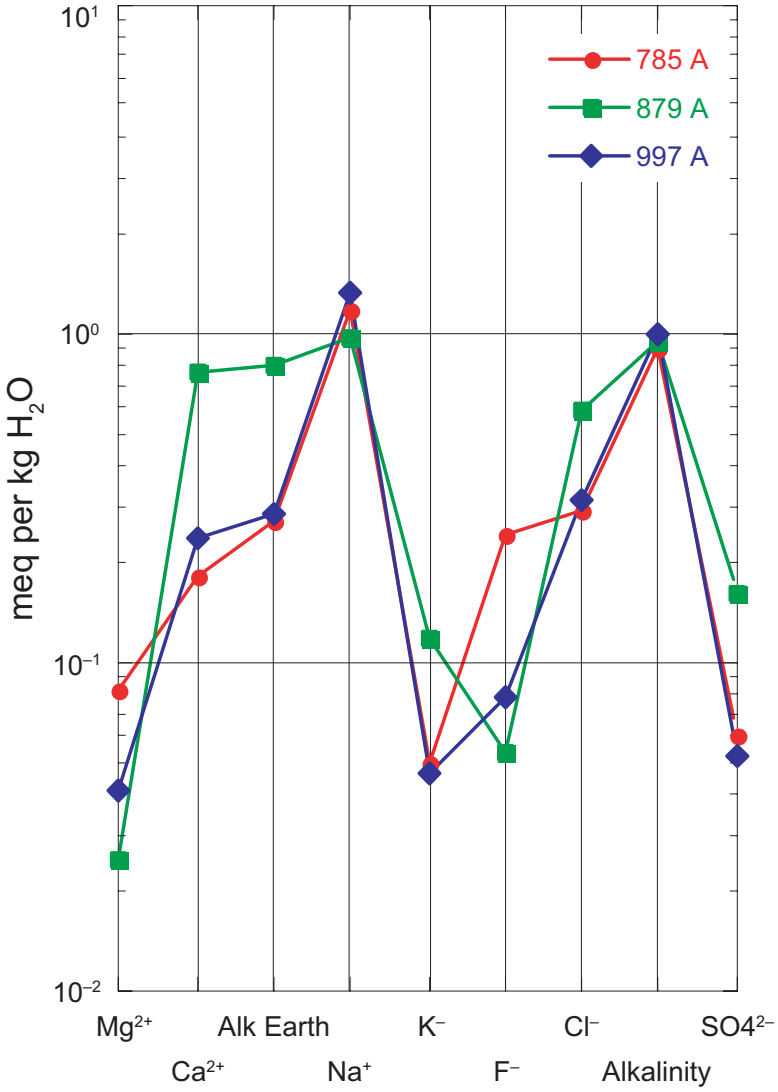

Figure 5-5. *Schoeller-diagram of the test solutions from the diffusion experiments after 133 days of diffusion time. Note the similar concentration pattern (except for F^-) for samples 785 A and 997A, both being different from that of sample 879 A.*

Table 5-5. Chemical composition and modelling data of the diffusion experiment test solutions.

Sample description				
Borehole		**KSH02**	**KSH02**	**KSH02**
Sample		785 A	879 A	997 A
Interval		785.30–785.52	879.28–879.53	997.01–997.26
Rock type		Fine-grained dioritoid	Fine-grained dioritoid	Fine-grained dioritoid
Type of sample		Aq Extract	Aq Extract	Aq Extract
Laboratory analytics		HI/UniBe	HI/UniBe	HI/UniBe
Laboratory extract		UniBe	UniBe	UniBe
Start experiment		Aug 06, 2003	Aug 06, 2003	Aug 06, 2003
End experiment		Nov 28, 2003	Nov 28, 2003	Nov 28, 2003
Experiment time		113 days	113 days	113 days
Miscellaneous properties				
pH (lab)	$-\log(H^+)$	6.99	7.22	7.21
Pt elec potent. vs SHE	mV			
Sample temperature	ºC	20	20	20
Dissolved constituents				
Cations				
Sodium (Na^+)	mg/L	27.3	22.1	30.9
Potassium (K^+)	mg/L	1.9	4.6	1.8
Magnesium (Mg^{+2})	mg/L	1.0	0.3	< 0.5
Calcium (Ca^{+2})	mg/L	3.7	15.5	4.8
Strontium (Sr^{+2})	mg/L	< 0.2	< 0.2	< 0.2
Anions				
Fluoride (F^-)	mg/L	4.6	1.0	1.5
Chloride (Cl^-)	mg/L	15.9	24.7	17.0
Bromide (Br^-)	mg/L	< 2.0	< 2.0	< 2.0
Sulphate (SO_4^{-2})	mg/L	2.9	7.9	2.5
Nitrate (NO_3^-)	mg/L	2.6	< 2.5	< 2.5
Total alkalinity	meqLl	0.90	0.95	1.0
Tot alkalinity as HCO_3	mg/L	54.9	58.0	61
Parameters calculated from analytical data				
Sum of anal. constit	mg/L	109	133	117
Charge balance	%	–1.04	+2.17	+5.92
Ion-Ion ratios				
Na/Cl molal	mol/mol	4.087	1.631	4.293
K/Na molal	mol/mol	0.041	0.122	0.034
SO_4/Cl molal	mol/mol	0.104	0.140	0.083
Carbonate system and saturation indeces				
Calculated using measured values				
TIC from alkalinity	mol/kg	1.111E–03	1.079E–03	1.140E–03
log p(CO_2)		–2.27	–2.48	–2.44
Calcite		–2.12	–1.26	–1.74
Dolomite		–4.52	–3.95	–4.18
Fluorite		–0.73	–1.46	–1.60
Gypsum		–4.25	–3.13	–4.10
Celestine		–4.97	–3.54	–4.80

Nevertheless certain indications can be drawn from these experiments for the *in-situ* pore water composition. The low Mg contents in all test solutions indicate that dissolution of hornblende, augitic pyroxene and biotite is very limited. Therefore the main source for dissolved potassium is K-feldspar, for dissolved sodium it is plagioclase, and for dissolved calcium are calcite and anorthite-rich plagioclase. The K contents in the test solutions of samples 785A and 997A are low (< 2 mg/L); the amount of feldspar dissolution in these samples seems limited. Together with the observed Na/Cl ratios far above unity it can be concluded that the larger proportion of this dissolved Na stems from the pore water and not from mineral dissolution. This suggests that Cl is not the only dominant anion in solution and the pore water of these samples might not be of a pure Na-Cl type.

A slightly different picture arises for sample 878A. The test solution of this sample shows high concentrations of Ca, SO_4 and K. The ratios of Na/Cl, K/Na, and SO_4/Cl compare to those of the aqueous extract solution of the two coarsest grain-size fractions (Tables 5-5 and 5-1). As for the aqueous extract solutions this suggests that the sulphuric acid produced from mineral sulphide dissolution could not be fully buffered by calcite dissolution, but also induced a significant amount of alumino-silicate dissolution. Because of the sluggish dissolution kinetics, these latter reactions advanced to a larger degree in the diffusion experiments compared to the aqueous extract solution. The low contents of Mg in both types of experimental solutions suggest that the dissolved alumino-silicates are mainly feldspars.

For all solutions it appears that during the experiment there exists no solubility control for either element by secondary mineral formation as indicated by the undersaturation of the solutions with respect to all mineral phases (Table 5-5).

5.3.3 Isotopic composition

In the diffusion experiments it was also attempted to obtain information about the isotopic composition of the pore water. The test solution used was free of chloride and the measured $\delta^{37}Cl$ thus essentially reflects that of the pore water as long as no significant fractionation took place during diffusion of Cl. Such fractionation processes are known to occur in claystones /e.g. Waber et al. 2001; Coleman et al. 2003; Gimmi and Waber, 2003/, but have not yet been shown for crystalline rocks. In case of an identical pore water signature a similar effect on the $\delta^{37}Cl$ in all test solutions would be expected because of the similar rock physical properties and the same experimental conditions. The large differences in $\delta^{37}Cl$ values obtained for the three test solutions (Table 5-5), however, suggest that the pore waters differ significantly in their chlorine isotope signature.

The test solution used was also free of strontium. However, mineral dissolution (calcite, feldspars etc) will also release Sr into the test solution. This Sr most probably will have a significantly different, yet unknown, Sr-isotope signature. The total Sr concentrations in samples 785A and 997A are 11 and 20 ppb, respectively, and that of sample 879A is 119 ppb. In the previous section it has been noted that mineral dissolution reactions were most prominent in the test solution of sample 879A. Therefore, this sample can be expected to have the largest proportion of Sr derived from mineral dissolution. Interestingly, the $^{87}Sr/^{86}Sr$ ratio measured for this sample is identical to that of the aqueous extract solution from the coarsest grain-size fractions, but much less radiogenic compared to the aqueous extract solution from the fine-grained grain-size fractions (Tables 5-5 and 5-1). This suggests that the influence of Sr from mineral dissolution is minimal and the $^{87}Sr/^{86}Sr$ ratio of the diffusion experiment test solution essentially reflects pore water ratios. Accepting this, the three pore water composition would have significantly different Sr-isotope ratios (Table 5-5).

In support of the diffusive-exchange experiments it was further attempted in the diffusion experiments to obtain information about the oxygen and hydrogen isotope composition of the pore water. This was done by spiking the test solutions with pure water depleted in ^{18}O and ^{2}H. By comparing the volumetric ratio of pore water present in the rock sample to that of the test solution (Table 5-3) it becomes obvious that the isotopic composition chosen for the test solution (Table 5-5) is far to less different compared to the range of pore water $\delta^{18}O$ and $\delta^{2}H$ values that could be expected /e.g. ranges given by Laaksoharju and Wallin, 1997/ and /Laaksoharju et al. 1999/. In addition, the experimental water appeared to have suffered evaporation during storage prior to analysis as can be seen from the less negative $\delta^{18}O$ and $\delta^{2}H$ values obtained compared to the test solutions after the experiment (Table 5-5). Therefore, the values obtained for the latter solutions cannot be interpreted.

Table 5-5. Isotopic data of the diffusion experiment test solutions.

Sample description					
Borehole			**KSH02**	**KSH02**	**KSH02**
Sample		Exp water	785 A	879 A	997 A
Interval			785.30–785.52	879.28–879.53	997.01–997.26
Rock type			Fine-grained dioritoid	Fine-grained dioritoid	Fine-grained dioritoid
Type of sample		Dist water	Diff-ex solut	Diff-ex solut	Diff-ex solut
Laboratory analytics		HI	HI/Waterl/UniBe	HI/Waterl/UniBe	HI/Waterl/UniBe
Laboratory experim		UniBe	UniBe	UniBe	UniBe
Start experiment		Aug 06, 2003	Aug 06, 2003	Aug 06, 2003	Aug 06, 2003
End experiment		Nov 28, 2003	Nov 28, 2003	Nov 28, 2003	Nov 28, 2003
Experiment Time	days	113	113	113	113
Isotopes					
$\delta^{18}O$ [1)]	‰V-SMOW	–18.83 ± 0.15	–18.91 ± 0.15	–18.84 ± 15	–18.83 ± 0.15
$\delta^{2}H$ [1)]	‰V-SMOW	–140.0 ± 1.5	–142.8 ± 1.5	–141.9 ± 1.5	–145.4 ± 1.5
$\delta^{37}Cl$	‰V-SMOC	Cl-free	2.92 ± 0.15	1.31 ± 0.15	1.74 ± 0.15
$^{87}Sr/^{86}Sr$	ratio	Sr-free	0.718975	0.724470	0.717874
$^{87}Sr/^{86}Sr$ error			± 0.00009	± 0.00002	± 0.00005
Sr ppm		Sr-free	0.011	0.119	0.020

[1)] values in italics are not trustworthy due to evaporation of the sample

5.4 Derivation of pore water composition

Assuming equilibrium between pore water and rock, a pore water composition can be calculated by applying geochemical modelling strategies in combination with diffusion experiments and an accurate measure of the water content in a rock sample. The equilibrium assumption between pore water and rock cannot be tested with the indirect pore water characterisation methods presented in this study, but have to be implied from measurements of the rock hydraulic properties, the distance to water-conducting zones, and the residence time of water circulating in such zones. At present such information is not available for the KSH02 borehole.

In such type of modelling an important parameter to know is the approximate ionic strength of the *in-situ* pore water. The reason for this is because every mineral equilibria depend on the ionic strengths of the solution. In most old formation waters the chemically conservative chloride is the most abundant anion and it is thus convenient to use chloride as an indicator for the ionic strength of the pore water.

5.4.1 Salinity

By knowing the exact water content of a rock, the concentration of Cl (or any other chemically conservative element) from a diffusion experiment can be calculated in a first approximation using the mass balance relation:

$$c_{pw} = \frac{\left[\left(m_{pw} + m_{tw}\right)\times c_{tw}\big|_{t=\infty} - \left(m_{tw} \times c_{tw}\big|_{t=0}\right)\right]}{m_{pw}} \qquad (8)$$

where c_{pw} = *in-situ* pore water concentration, m_{pw} = mass of pore water (water content), m_{tw} = mass test water, c_{tw} = Cl concentration of test water before the experiment (t = 0) and at steady state conditions (t = ∞). This approximation is valid as long as steady state conditions are achieved and the pore water to test-water ratio is very low in the experiment. As shown in Table 5-3, this ratio was below 0.005 in the present experiments and thus has no influence on the above mass balance.

From equation (8) in becomes obvious that the water content of the rock sample is the most important parameter besides the Cl concentration measured in the test solution. The larger the absolute water content the less is the influence of the error attached with the water content on the calculated Cl concentration of the pore water. As discussed in Section 4.2.2, the gravimetric determination of the water content is associated with large uncertainties due to the desaturation evident when the samples were received; this is due to stress release effects. Unfortunately, the degree of saturation also affects the derivation of the water content by the diffusive-exchange method (cf Section 5.2), the approach which is independent of drying and gravimetry. Therefore, the Cl content of the *in-situ* pore water can only be estimated within a range and attached with a rather large uncertainty. Table 5-6 gives the best estimate (average) together with minimum and maximum values of the *in-situ* Cl concentration as based on the present data given in Table 5-6. *It appears that the Cl content of the pore water in the quartz monzodiorite rocks of borehole KSH02 increases between 785 m and 997 m depth from about 5,000 mg/L to about 7,100 mg/L (Figure 5-6).*

Table 5-6. Estimates of the range of the *in-situ* pore water Cl content based on diffusion experiments and different water content measurements (see text).

Sample KSH02-	Mass rock (g)	Mass test water (g)	Water content (%)	Mass pore water (g)	Initial Cl test water (mg/kgH_2O)	Final Cl test water (mg/kgH_2O)	Cl pore water (mg/kgH_2O)
Error [1]	± 5%	± 5%	stdev.	cumulative		± 5%	cumulative
785 A							
average	449.02	121.92	0.085	0.38	0	15.9	5,075
max [2]	426.57	115.82	0.069	0.30		16.7	6,559
min [2]	471.47	128.02	0.101	0.48		15.1	4,061
879 A							
average	420.76	132.24	0.119	0.50	0	24.7	6,512
max [2]	399.72	125.63	0.115	0.46		25.9	7,104
min [2]	441.80	138.85	0.124	0.55		23.5	5,962
997 A							
average	407.43	114.56	0.067	0.28	0	17.0	7,089
max [2]	387.06	108.83	0.060	0.23		17.9	8,422
min [2]	427.80	120.29	0.075	0.32		16.2	6,048

[1] relative error for weight measurements and Cl analysis, standard deviation of multiple measurements for water content (Table 4-5), and cumulative error for mass of pore water and pore water Cl-content.

[2] max = positive error on weight measurements, negative error on Cl analysis; min = negative error on weight measurements, positive error on Cl analysis.

5.4.2 Isotopic composition

In contrast to the concentrations of dissolved constituents in the pore water, the isotope ratios of such constituents are not changed during dilution as long as no mineral reactions take place. For the chemically conservative chloride no such mineral reactions occurred during the diffusion experiments and the $\delta^{37}Cl$ values are representative for *in-situ* pore water. Although less certain, the effect of mineral dissolution during the diffusion experiments with KSH02 core samples also appears to be negligible for the Sr-isotope ratio. This is based on the comparison of the chemical and isotopic data obtained from aqueous extraction and diffusion experiments (cf Section 5.3.3).

When plotted against the borehole depth of the samples (Figures 5-6 and 5-7) it appears that the pore water of the three samples is isotopically different and shows a similar stratification with depth as deduced for the salinity. Thus, in spite of all uncertainty attached to individual analytical and calculated data, the isotopic data of the pore water are in support of the different salinity of the pore water.

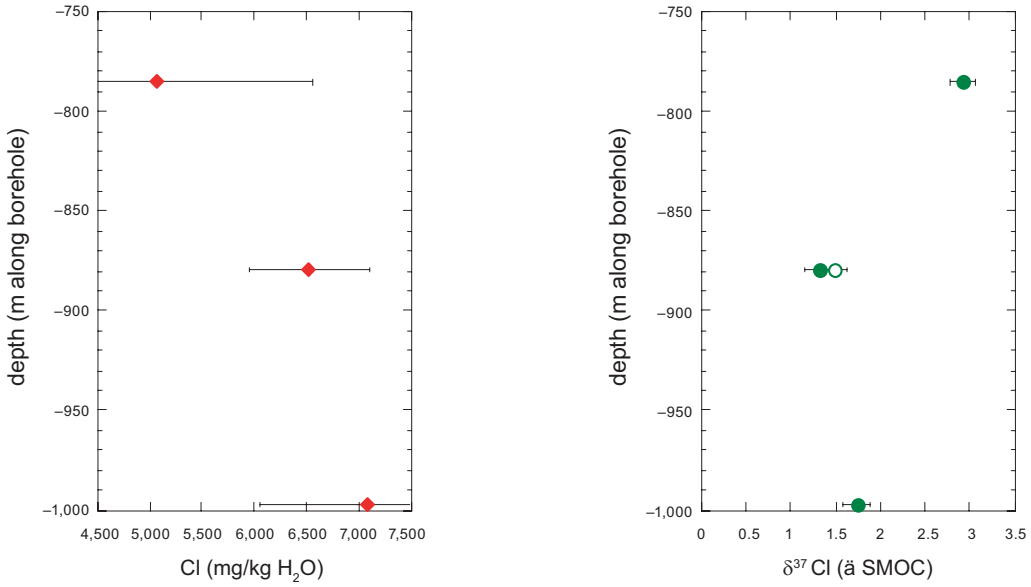

Figure 5-6. *Estimate of Cl contents in the in-situ pore water as derived from diffusion experiments (right) and the Cl-isotope composition of the in-situ pore water (left). For sample KSH02-879 the test solutions of the diffusion experiment (closed symbol) and the aqueous extraction of the most coarse-grained grain-size fraction (open symbol) have identical $\delta^{37}Cl$ values.*

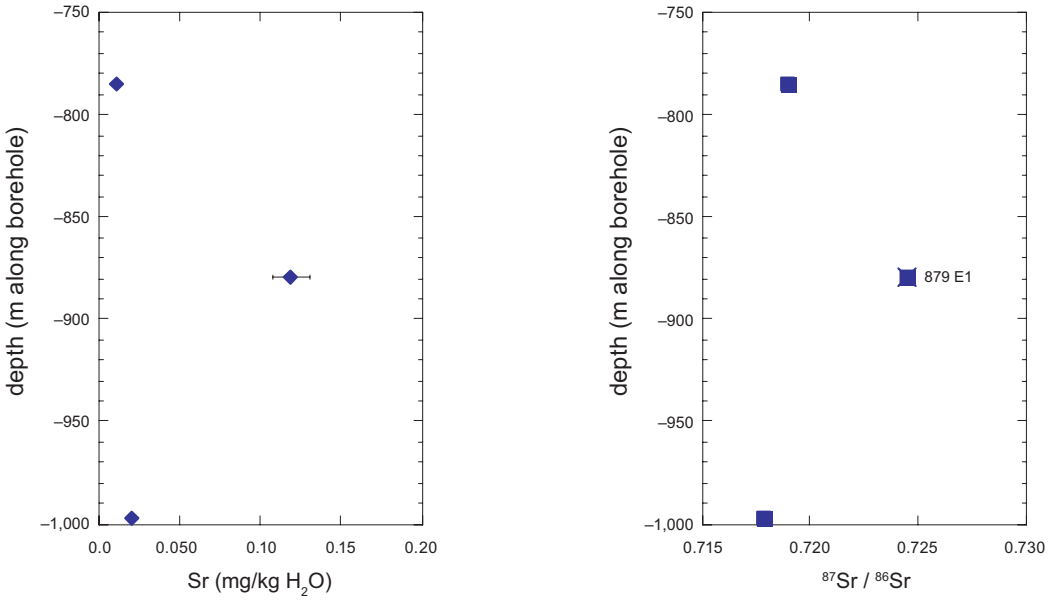

Figure 5-7. *Sr contents (right) and Sr-isotope ratios (left) in the test solutions from the diffusion experiments. For sample KSH02-879 the Sr-isotope ratios of the test solutions of the diffusion experiment (closed symbol) and the aqueous extraction of the most coarse-grained grain-size fraction (cross) are identical suggesting that mineral dissolution is negligible and the Sr-isotope ratios are representative for in-situ pore water.*

6 Summary and conclusions

Different diffusive equilibration techniques have been applied on three core samples from borehole KSH02. Such indirect methods for the chemical characterisation of *in-situ* pore water in rocks of low permeability can only provide parts of the pore water chemistry and have to be applied in conjunction with geochemical modelling to derive the complete chemical composition. Modelling of the composition requires, in addition, information about the mineralogy, porosity, mineral fluid inclusions, and aqueous extraction behaviour of the rocks. In addition, the equilibrium state of the pore water with the surrounding rocks needs to be defined based on hydrochemical and hydrological investigations of the water-conducting zones in the rock body.

The three samples from 785 m, 879 m, and 997 m of depth along borehole KSH02 are of fine-grained dioritoid composition with a chemical composition typical for such rocks. The rocks display only weak deformation and hydrothermal alteration phenomena. An oxidising alteration is absent. They consist of a fine-grained matrix with phenocrysts of feldspars, amphibole (hornblende), pyroxene (augite) and biotite. Plagioclase and K-feldspar are the most abundant minerals followed by amphibole, quartz, biotite, pyroxene, and opaque phases. This mineralogy together with secondary phases such as calcite and chlorite controls the pore water composition. Quartz contributes between 10 to 20 vol % of the rocks and contains 0.5 to 1 vol % of the total fluid inclusions. The most abundant fluid inclusions are secondary, two-phase inclusions with a salinity between about 1 and 25 eq wt % NaCl. $CaCl_2$ is present in variable amounts in inclusions with more than about 6 eq wt % NaCl . Less abundant are CO_2-rich gas-only inclusions of probably primary origin. Combined with aqueous extraction tests the fluid inclusions studies revealed that the fluid inclusions form a significant source of salinity and also CO_2 in the case of inclusion leakage.

Diffusion experiments and the diffusive-exchange method for determination of the Cl content, the stable isotope composition and the water content were successfully applied although the results are not accurate enough for modelling of the complete pore water composition. The reason for this is the desaturation of the rock samples between the time of recovery and their arrival at the laboratory. While this desaturation essentially inhibits gravimetric water content determinations, it also affects the diffusive-exchange method by Rayleigh-distillation effects. This latter technique was applied for the first time to crystalline rocks in order to overcome perturbation of the gravimetric water content measurements induced by stress release of the rock. Stress release was identified to be significant during re-saturation of the rock samples.

In spite of these limitations induced by desaturation it appears that the pore water in the KSH02 borehole is chemically and isotopically stratified between 785 m and 997 m depth. Chloride concentrations appear to increase from about 5,000 mg/L to 7,100 mg/L and the pore water has different chlorine and strontium isotopic signatures. This implies a complex palaeohydrogeological evolution in the more recent past (10^4 to 10^5 years) because in a system that has been stable over long periods of time a homogenised pore water would be expected over such short distances.

7 References

Araguàs-Araguàs L, Rozanski K, Gonfiantini R, Louvat D, 1995. Isotope effects accompanying vacuum extraction of soil water for stable isotope analyses. J. Hydrol., 168, 159–171.

Clark I D, Fritz P, 1997. Environmental isotopes in hydrogeology. Lewis Publishers, Boca Raton, FL, USA.

Coleman M, Isaac M, Thornley D, 2003. Stable Chlorine Isotopic Analysis. Annex 7 in Pearson et al. 2003a, Mont Terri Project – Geochemistry of Water in the Opalinus Clay Formation at the Mont Terri Laboratory. Reports of the Federal Office of Water and Geology (FOWG), Geology Series No 5, Bern, Switzerland, 263–268.

Eliasson T, 1993. Mineralogy, geochemistry and petrophysics of red coloured granite adjacent to fractures. SKB TR-93-06, Svensk Kärnbränslehantering AB, 68 p.

Gimmi T, Waber H N, 2003. Modelling of profiles of stable water isotopes, chloride and chlorine isotopes of pore water in argillaceous rocks in the Benken borehole. Unpubl. Nagra Internal Report, Wettingen, Switzerland, 71 p.

Horita J, Wesolowski D J, Cole D R, 1993. The activity-composition relationship of oxygen and hydrogen isotopes in aqueous salt solutions: I. Vapor-liquid water equilibration of single salt solutions from 50 to 100°C. Geochim. Cosmochim. Acta 57, 2,797–2,817.

Laaksoharju M, Wallin B (eds), 1997. Evolution of the groundwater chemistry at the Äspö Hard Rock Laboratory: Proceedings of the Äspö International Geochemistry Workshop, June 6–7, 1995. SKB ICR-97-04, Svensk Kärnbränslehantering AB.

Laaksoharju M, Tullborg E-L, Wikberg P, Wallin B, Smellie J A T, 1999. Hydrogeochemical conditions and evolution of the Äspö HRL, Sweden. Appl. Geochem., 14, 819–834.

Moreau-Le Golvan Y, Michelot J-L, Boisson, J-Y, 1997. Stable isotope contents of pore water in a claystone formation (Tournemire, France): assessment of the extraction technique and preliminary results. Appl. Geochem. 12, 739–745.

Pearson F J, 1999. What is the porosity of a mudrock? In: Aplin, A.C., Fleet, A.J., & Macquaker, J.H.S., (eds.), Muds and Mudstones: Physical and Fluid Flow Properties. London, Geol. Soc. Spec. Publ. 158, 9–21.

Pearson F J, Arcos D, Bath A, Boisson J-Y, Fernández A M, Gäbler H-E, Gaucher E, Gautschi A, Griffault L, Hernán P, Waber H N, 2003a. Mont Terri Project – Geochemistry of Water in the Opalinus Clay Formation at the Mont Terri Laboratory. Reports of the Federal Office of Water and Geology (FOWG), Geology Series No 5, Bern, Switzerland, 319 p.

Pearson F J, Fernández A M, Gaboriau H, Waber H N, Bath A, 2003b. Porosity and Water Content of Mont Terri Claystones. Appendix 10 in Pearson et al. 2003a, Mont Terri Project – Geochemistry of Water in the Opalinus Clay Formation at the Mont Terri Laboratory. Reports of the Federal Office of Water and Geology (FOWG), Geology Series No 5, Bern, Switzerland, 304–319.

Rogge T, 1997. Eine molekular-diffusive Methode zur Bestimmung des Porenwassergehaltes und der Zusammensetzung von stabilen Isotopen im Porenwasser von Gestein. Unpubl. Diploma Thesis, Institut für Umweltphysik, Unversity of Heidelberg, 76 p.

Rübel A P, 2000. Stofftransport in undruchlässigen Gesteinsschichten – Isotopenuntersuchungen im Grund- und Porenwasser. PhD Thesis, Institut für Umweltphysik, Unversity of Heidelberg, Der Andere Verlag, Osnabrück, Germany, 184 p.

Rübel A P, Sonntag Ch, Lippmann J, Pearson F J, Gautschi A, 2002. Solute transport in formations of very low permeability: Profiles of stable isotope and dissolved noble gas contents of pore water in the Opalinus Clay, Mont Terri, Switzerland. Geochim. Cosmochim. Acta, 1,311–1,321.

Sacchi E, Michelot J-L, 2000. Porewater Extraction from Argillaceous Rocks for Geochemical Characterisation. Methods and Interpretation. Paris, OECD Nuclear Energy Agency, 185 p.

Sacchi E, Michelot J-L, Pitsch H, Lalieux P, Aranyossy F-J, 2001: Extraction of water and solutes from argillaceous rocks for geochemical characterisation: Methods, processes, and current understanding. Hydrogeology Journal, 9, 17–33.

Smellie J A T, Waber H N, Frape S K, 2003. Matrix fluid chemistry experiment, Final Report. SKB TR-03-18, Svensk Kärnbränslehantering AB, 162 p.

Sverdrup H U, 1990. The kinetics of base cation release due to chemical weathering. Lund University Press, Lund, Sweden, 246 p.

Waber H N, Frape S K, Gautsch A, 2001. Cl-isotopes as Indicator for a Complex Paleohydrogeology in Jurassic Argillaceous Rocks, Switzerland. In Cidu, R. (ed.): Water-Rock Interaction: Proc. 10th Internat. Symp. on Water-Rock Interaction – WRI-10, Villasimius, Italy, Lisse, The Netherlands, A. A. Balkema, p 1,403–1,406.

Appendix

Documentation of the fluid inclusion study

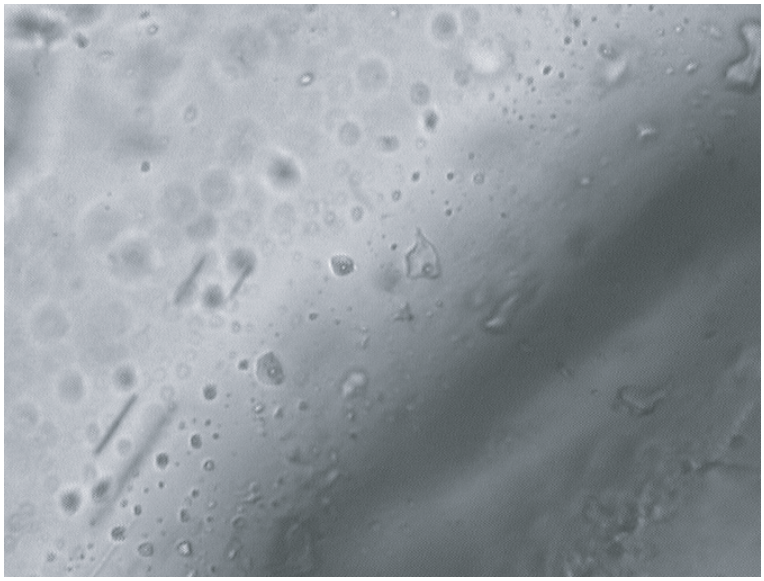

Figure A-1. *Association of two-phase liquid-vapour fluid inclusion in quartz. The three inclusions with the vapour bubble belong to Type Ic with a salinity of about 16 eq wt % NaCl (sample 785F, inclusion no 1.1.1 to 1.1.3, cf Table A1).*

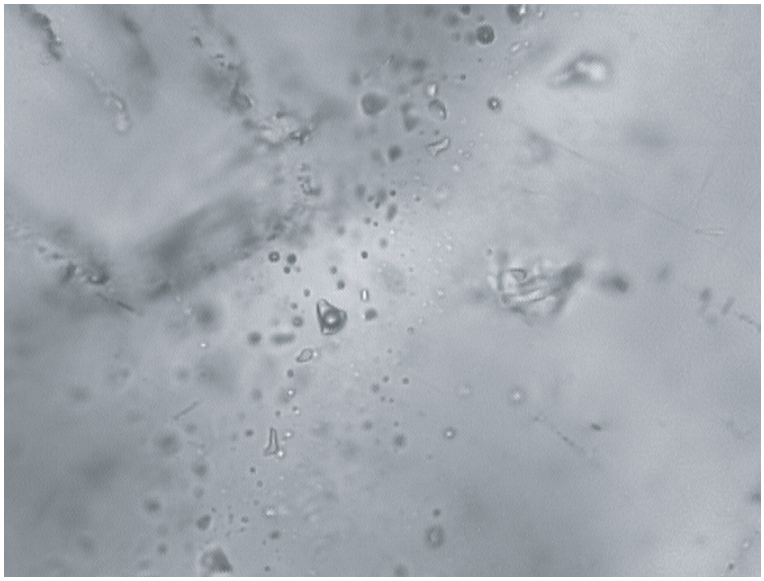

Figure A-2. *Two-phase liquid-vapour inclusion surrounded by single phase liquid inclusions. The two-phase inclusion belongs to Type 1a with a salintiy of 0.2 eq wt % NaCl (sample 785F, inclusion no 2.0.6, cf Table A-1).*

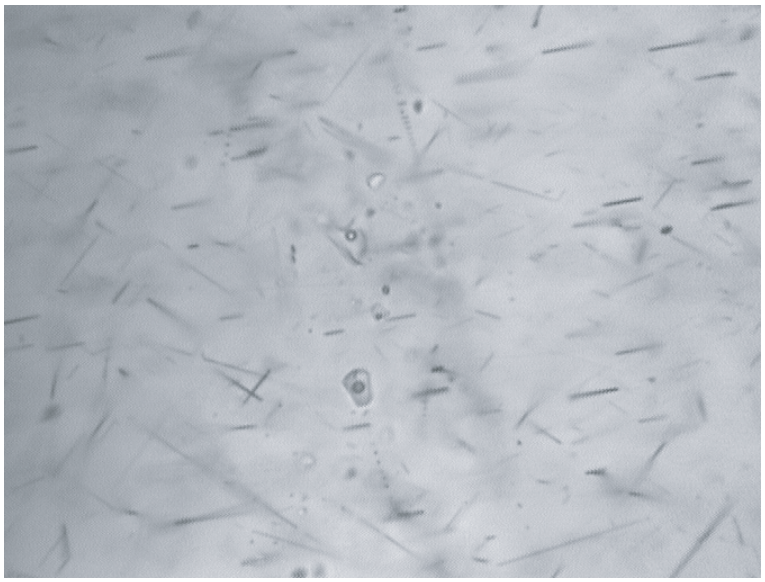

Figure A-3. *Two-phase liquid-vapour inclusions of Type Ic in sample 785 F. Inclusion no 3.1.4 (top) has a melting temperature for ice of –26.7°C what disables the calculation of a salinity as eq wt % NaCl, but indicates a very high salinity. Inclusion no 3.1.5 (bottom) yields a salinity of 20.2 eq wt % NaCl.*

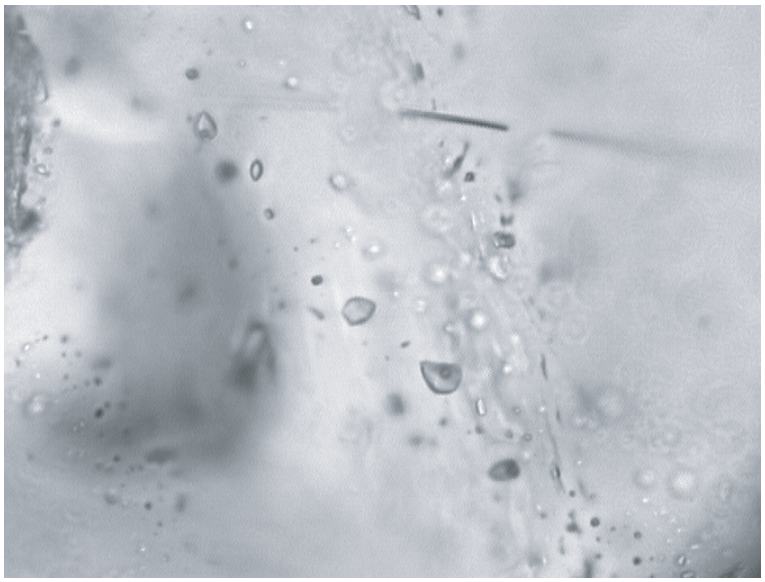

Figure A-4. *Trail of two-phase liquid-vapour inclusions of Type Ib along a healed fissure in sample 879 F. The salinity of the inclusions is between 7 and 8 eq wt % NaCl (inclusion no 879F 3.3.10 and 3.3.11 in Table A-2).*

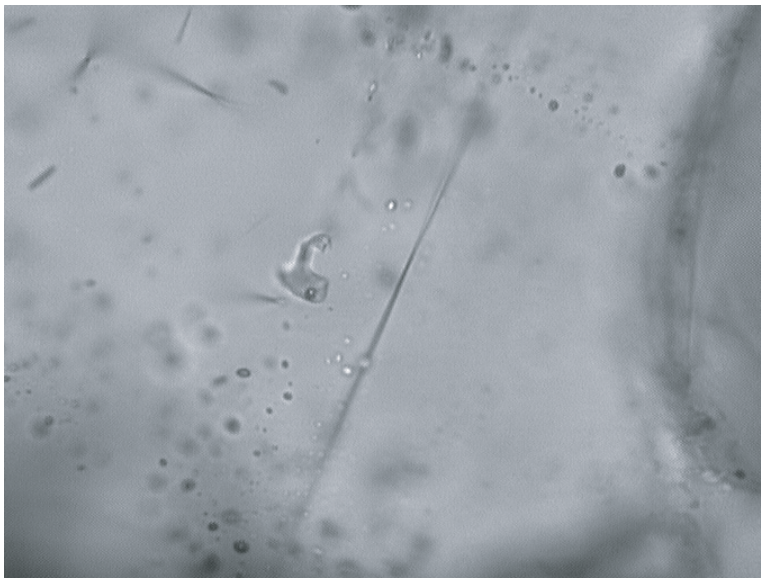

Figure A-5. *Two-phase liquid-vapour inclusions of Type Ic in sample 997 F. The inclusion has a salinity of 22.4 eq wt % NaC. Based on phase stability relationship, and Raman investigation of hydrohalite decomposition the salinity s composed of about 16 wt % $CaCl_2$ and only 5 wt % of NaCl (inclusion no 997F 3.6.23, cf Figure A-6 and Tables A-3 and 4-4 in the text).*

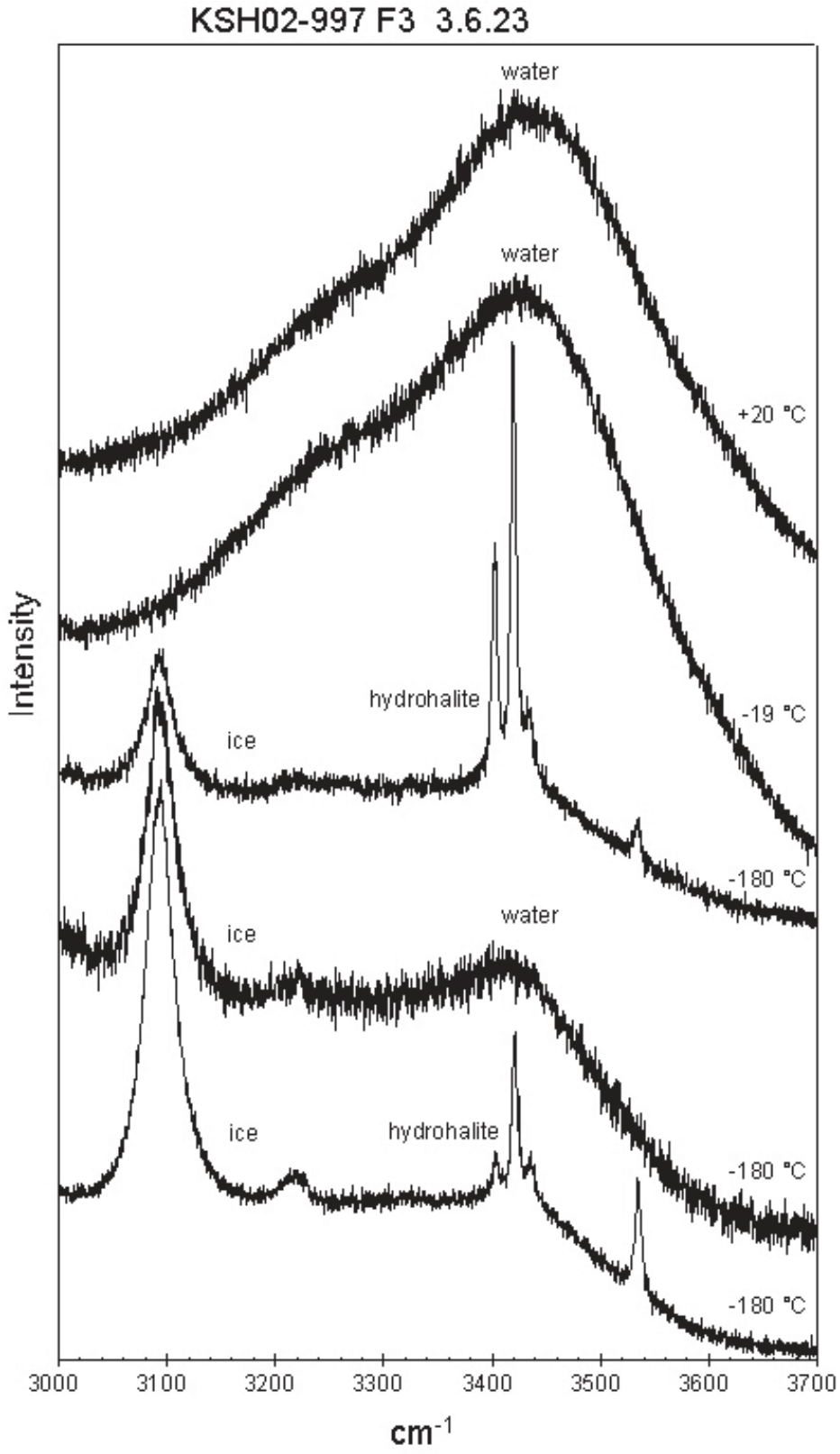

Figure A-6. *Variation of Raman spectra as a function of temperature of inclusion no 3.6.23 of sample 997 F. The decomposition of hydrohalite was observed to occur between –31°C and –32°C indicating a salt composed of $CaCl_2$ and NaCl. No other salt hydrates are observed in the Raman spectra (cf Figure A-5, Tables A-3 and 4-4 in the text).*

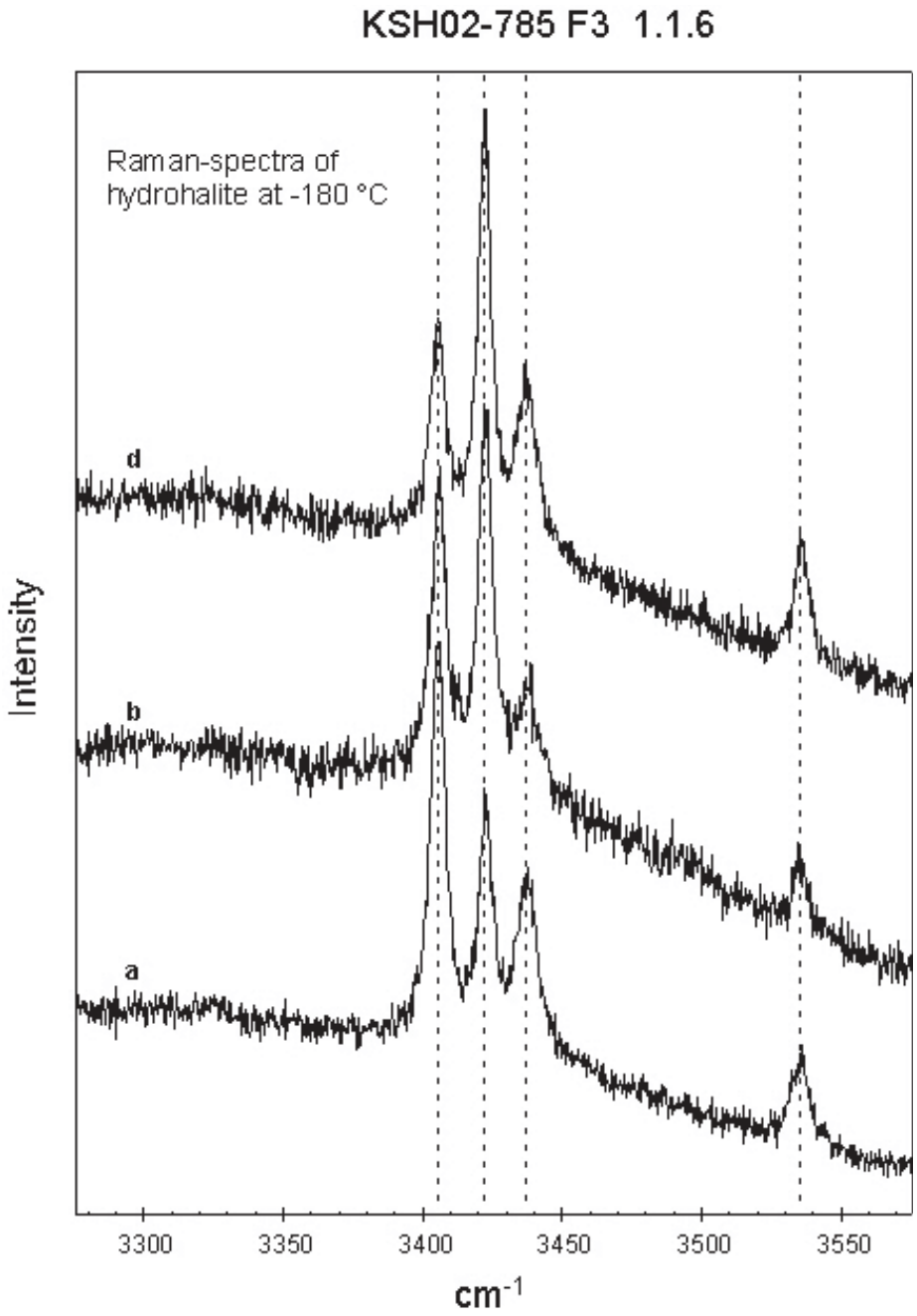

Figure A-7. *Raman spectra of inclusion no 1.1.6 of sample 785 F. The decomposition of hydrohalite was observed to occur between –27ºC and –28ºC indicating a salt composed of $CaCl_2$ and NaCl. No other salt hydrates are observed in the Raman spectra (cf Tables A-1 and 4-4 in the text).*

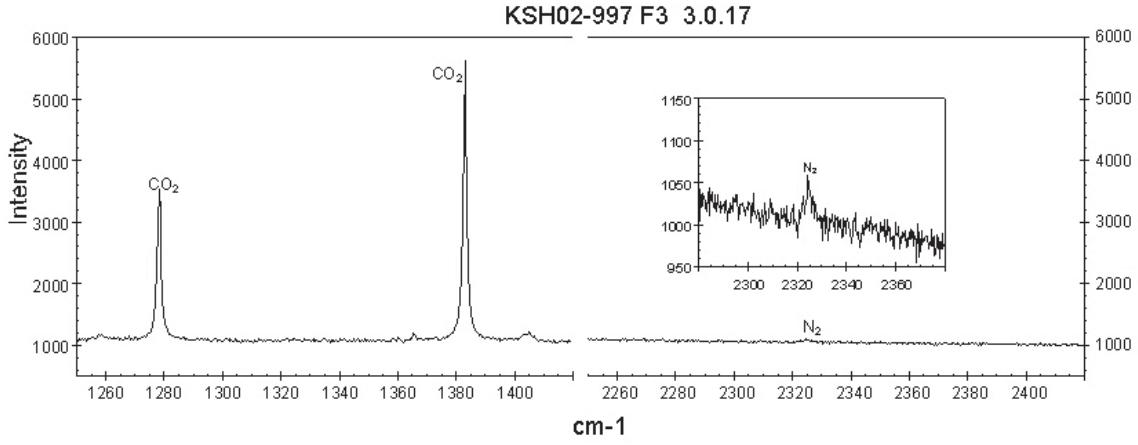

Figure A-8. *Raman spectra of single-phase gas-only inclusion no 3.0.17 of sample 997 F. Thegas phase is almost entirely made of CO_2 (cf Tables A-4 and 4-2 in the text).*

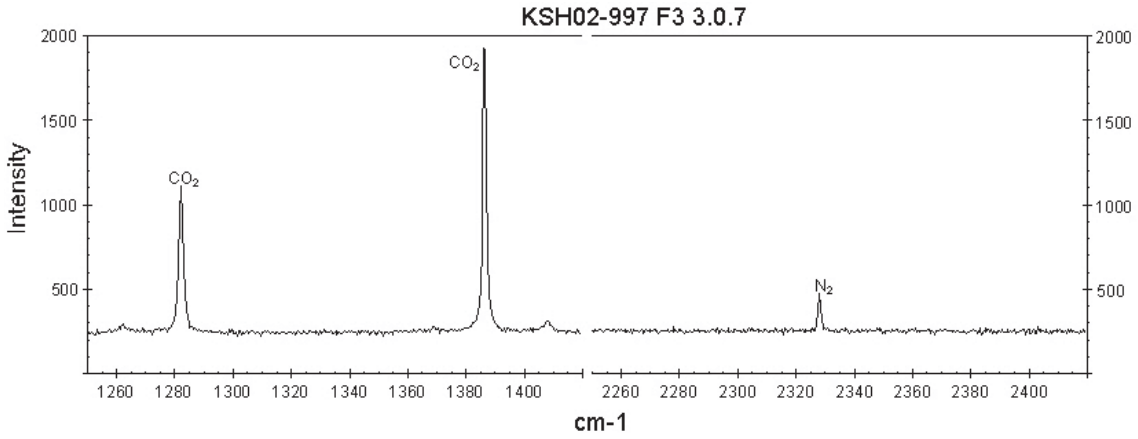

Figure A-9. *Raman spectra of single-phase gas-only inclusion no 3.0.7 of sample 997 F. Thegas phase is mainly made of CO_2 with traces of N_2 (cf Tables A-4 and 4-2 in the text).*

Table A-1. Microthermometry of fluid inclusions in quartz of sample 785 F.

FI Number	Assemblage	Type	Origin	Phases	Tn ice (°C)	Tm ice (°C)	Salinity (eq wt % NaCl)
1.1.1	1	Ic	second	L + V	–63.0	–12.9	16.8
1.1.2	1	Ic	second	L + V	–62.3	–12.9	16.8
1.1.3	1	Ic	second	L + V	–62.1	–12.7	16.7
1.1.4	1	Ic	second	L + V	–62.0	–13.0	16.9
1.1.5	1	Ic	second	L + V	–65.5	–14.6	18.3
1.1.6	1	Ic	second	L + V	–62.5	–13.2	17.1
1.1.7	1	Ic	second	L + V	–62.5	–12.9	16.8
1.1.8	1	Ic	second	L + V	–62.0	–12.5	16.5
1.2.9	2	Ib	second	L + V	–50.7	–6.6	10.0
1.2.10	2	Ib	second	L + V	–50.0	–6.1	9.4
1.2.11	2	Ic	second	L + V	–49.3	–10.1	14.1
1.2.12	2	Ib	second	L + V	–53.9	–8.3	12.1
2.1.1	2	Ia	second	L + V	–40.7	–0.9	1.6

FI Number	Assemblage	Type	Origin	Phases	Tn ice (°C)	Tm ice (°C)	Salinity (eq wt % NaCl)
2.1.2	2	Ia	second	L + V	–40.2	–0.6	1.0
2.1.3	2	Ia	second	L + V	–40.6	–0.8	1.4
2.2.4	2	Ib	second	L + V	–50.4	–6.4	9.7
2.2.5	2	Ib	second	L + V	–51.0	–6.5	9.9
2.0.6	none	Ia	second	L + V	–29.4	–0.1	0.2
2.0.7	none	Ib	second	L + V	–54.4	–8.1	11.9
2.0.8	none	Ib	second	L + V	–48.1	–5.2	8.1
2.0.9	none	Ib	second	L + V	–48.6	–6.1	9.4
2.0.10							
3.2.7	2	Ib	second	L + V	≈ –48	–4.8	7.6
3.2.8	2	Ib	second	L + V	n d	–3.8	6.1
3.0.9	none	Ia	second	L + V	–41.3	–1.5	2.6

Abbr: L = liquid, V = vapour, Tn ice = nucleation temperature of ice, Tm ice = final ice melting temperature, second = secondary inclusion, mst = metastable, n d = not determined, n.c = not calculated.

Bold: Composition further investigated with Raman-Spectrometry.

Table A-2. Microthermometry of fluid inclusions in quartz of sample 879 F.

FI Number	Assemblage	Type	Origin	Phases	Tn ice (°C)	Tm ice (°C)	Salinity (eq wt % NaCl)
1.1.1	1	Ib	second	L + V	–50.0	–5.7	8.8
1.1.2	1	Ib	second	L + V	–49.8	–5.7	8.8
1.1.3	1	Ib	second	L + V	–48.8	–5.3	8.3
1.1.4	1	Ib	second	L + V	–49.6	–5.5	8.6
1.1.5	1	Ib	second	L	n d	–4.3	6.9
1.2.6	2	Ib	second	L + V	–50.7	–6.9	10.4
1.2.7	2		second	L + V	–48.6	mst.	–
1.2.8	2	Ib	second	L	n d	–6.8	10.3
1.2.9	2	Ib	second	L + V	–54.0	–8.3	12.1
1.2.10	2	Ib	second	L + V	–53.0	–8.0	11.7
1.3.11	3	Ib	second	L + V	–47.3	–4.9	7.7
1.3.12	3		second	L + V	–46.5	mst.	–
1.3.13	3	Ib	second	L + V	–47.7	–5.0	7.9
1.3.14	3	Ib	second	L + V	–46.6	–4.1	6.6
1.3.15	3	Ib	second	L + V	–46.6	–4.0	6.4
1.4.16	4	Ib	second	L + V	–46.5	–4.1	6.6
1.4.17	4	Ib	second	L + V	–46.1	–4.0	6.4
1.0.18	none	Ib	second	L + V	–48.6	–5.6	8.7
2.1.1	1	Ib	second	L + V	–47.7	–4.6	7.3
2.1.2	1	Ib	second	L + V	–48.5	–5.4	8.4
2.1.3	1	Ib	second	L + V	–47.6	–4.7	7.4
2.1.4	1	Ib	second	L + V	–48.0	–4.9	7.7
2.1.5	1	Ib	second	L + V	–47.9	–5.1	8.0
2.1.6	1	Ib	second	L + V	–47.3	–4.7	7.4
2.1.7	1	Ib	second	L + V	–46.9	–4.6	7.3
3.1.1	1	Ic	second	L + V	–40.0	–1.0	1.7

FI Number	Assemblage	Type	Origin	Phases	Tn ice (°C)	Tm ice (°C)	Salinity (eq wt % NaCl)
3.1.2	1	Ic	second	L + V	–40.2	–1.0	1.7
3.1.3	1	Ic	second	L + V	–40.0	–0.9	1.6
3.1.4	1	Ic	second	L + V	–40.4	–1.0	1.7
3.2.5	2	Ib	second	L + V	–49.8	–5.7	8.8
3.2.6	2		second	L + V	–48.8	mst.	–
3.2.7	2	Ib	second	L + V	–48.5	–5.4	8.4
3.2.8	2	Ib	second	L + V	–48.7	–5.3	8.3
3.2.9	2	Ib	second	L + V	–47.7	–4.9	7.7
3.3.10	3	Ib	second	L + V	–47.6	–4.9	7.7
3.3.11	3	Ib	second	L + V	–46.7	–4.7	7.4

Abbr: L = liquid, V = vapour, Tn ice = nucleation temperature of ice, Tm ice = final ice melting temperature, second = secondary inclusion, mst = metastable, n d = not determined.

Bold: Composition further investigated with Raman-Spectrometry.

Table A-3. Microthermometry of fluid inclusions in quartz of sample 997 F.

FI Number	Assemblage	Type	Origin	Phases	Tn ice (°C)	Tm ice (°C)	Salinity (eq wt % NaCl)
1.2.2	2	–	second	L + V	–80.8	–22.0	n c
1.2.3	2	–	second	L + V	–98.0	–30.5	n c
1.2.4	2	–	second	L + V	–100.0	–33.6	n c
1.2.5	2	–	second	L + V	–91.0	–29.2	n c
1.2.6	2	–	second	L + V	–89.8	–27.3	n c
1.3.7	3	Ia	second	L + V	–41.9	–1.9	3.2
1.4.8	4	Ia	second	L + V	–41.9	–1.6	2.7
2.1.1	1	Ia	second	L + V	–43.0	–1.9	3.2
2.1.2	1	Ia	second	L + V	–40.9	–1.7	2.9
2.1.3	1	Ia	second	L + V	n d	–1.7	2.9
2.1.4	1	Ia	second	L + V	n d	–1.9	3.2
2.2.5	2	Ib	second	L + V	–44.6	–4.1	6.6
2.2.6	2	Ia	second	L + V	–44.0	–2.5	4.2
2.2.7	2	Ib	second	L + V	–47.0	–3.9	6.3
2.2.8	2	Ia	second	L + V	–41.6	–1.5	2.6
3.2.8	2	Ia	second	L + V	–44.5	–3.0	4.9
3.2.9	2	Ia	second	L + V	–45.1	–3.2	5.2
3.3.10	3	Ia	second	L + V	–43.2	–3.1	5.1
3.3.12	3	Ia	second	L + V	–44.3	–3.0	4.9
3.3.13	3	Ia	second	L + V	–44.8	–2.9	4.8
3.3.14	3	Ia	second	L + V	–41.1	–2.9	4.8
3.4.15	4	–	second	L + V	no ice nucl	no ice nucl	high
3.4.16	4	–	second	L + V	no ice nucl	no ice nucl	high
3.0.18	none	Ia	second	L + V	–44.4	–3.0	4.9
3.5.19	5	Ia	second	L + V	–44.9	–3.1	5.1
3.5.20	5	Ia	second	L + V	n d	–3.4	5.5
3.6.23	6	Ic	second	L + V	–74.8	–20.0	22.4
3.6.24	6	–	second	L + V	–95.0	–33.7	n c

4.1.1	1	Ia	second	L + V	–41.3	–1.6	2.7
4.1.2	1	Ia	second	L + V	–42.2	–1.8	3.0
4.1.3	1	Ia	second	L + V	–41.9	–1.7	2.9
4.2.4	2	–	second	L + V	no ice nucl	no ice nucl	high
4.2.5	2	–	second	L + V	no ice nucl	no ice nucl	high
4.3.6	3	Ia	second	L + V	–40.4	–1.1	1.9
4.3.7	3	Ia	second	L + V	–41.7	–1.6	2.7
4.3.8	3	Ia	second	L + V	–41.9	–1.5	2.6
4.0.9	none	Ib	second	L + V	–52.5	–7.3	10.9
4.0.10	none	Ic	second	L + V	–72.0	–19.0	21.7

Abbr: L = liquid, V = vapour, Tn ice = nucleation temperature of ice, Tm ice = final ice melting temperature, second = secondary inclusion, mst = metastable, n d = not determined, n c = not calculated.

Bold: Composition further investigated with Raman-Spectrometry.

Table A-4. Microthermometry of gas-only fluid inclusions in quartz of sample 997 F.

FI Number	Type	Origin	Phases	Tm CO_2 (°C)	Tn Clath (°C)	Tm Clath (°C)	Th CO_2 (°C)
3.0.4	II	prim.	V	–56.6	n d	n d	24.2 L
3.0.5	II	prim.	V	–56.7	n d	–7.5	25.3 L
3.0.6	II	prim.	V	–56.7	n d	n d	26.4 L
3.0.7	II	prim.	V	–57.9	n d	n d	9.2 L
3.0.11	II	prim.	V	n d	n d	8.0	25.0 V
3.0.17	II	prim.	V	–56.6	–30.7	–5.9	7.7 L

Abbr: V = vapour, Tm CO_2 = melting temperature of solid CO_2, Tn Clath = nucleation temperature of gas-hydrate, Tm Clath = melting temperature of gas-hydrate, Th CO_2 = homogenisation temperature of CO_2, L = CO_2 homogenisation into liquid phase, V = CO_2 homogenisation into gas phase, prim = primary inclusion, n d = not determined.

Bold: Composition further investigated with Raman-Spectrometry.